Contalactone, a contaminant formed during chemical synthesis of the strigolactone reference GR24 is also a strigolactone mimic

Alexandre de Saint Germain, Pascal Retailleau, Stéphanie Norsikian, Vincent Servajean, Franck Pelissier, Vincent Steinmetz, Jean-Paul Pillot, Soizic Rochange, Jean-Bernard Pouvreau, François-Didier Boyer

Highlights

- Characterization of (±)-contalactone, a contaminant of synthetic strigolactone GR24
- (±)-Contalactone inhibits branching in pea via RMS3/PsD14 strigolactone receptor
- (±)-Contalactone represses hypocotyl elongation in *Arabidopsis* via AtD14 and AtKAI2
- (±)-Contalactone is a potent germination stimulant of various root parasitic plants
- (±)-Contalactone induces the colonization of AM fungi in *Medicago truncatula*

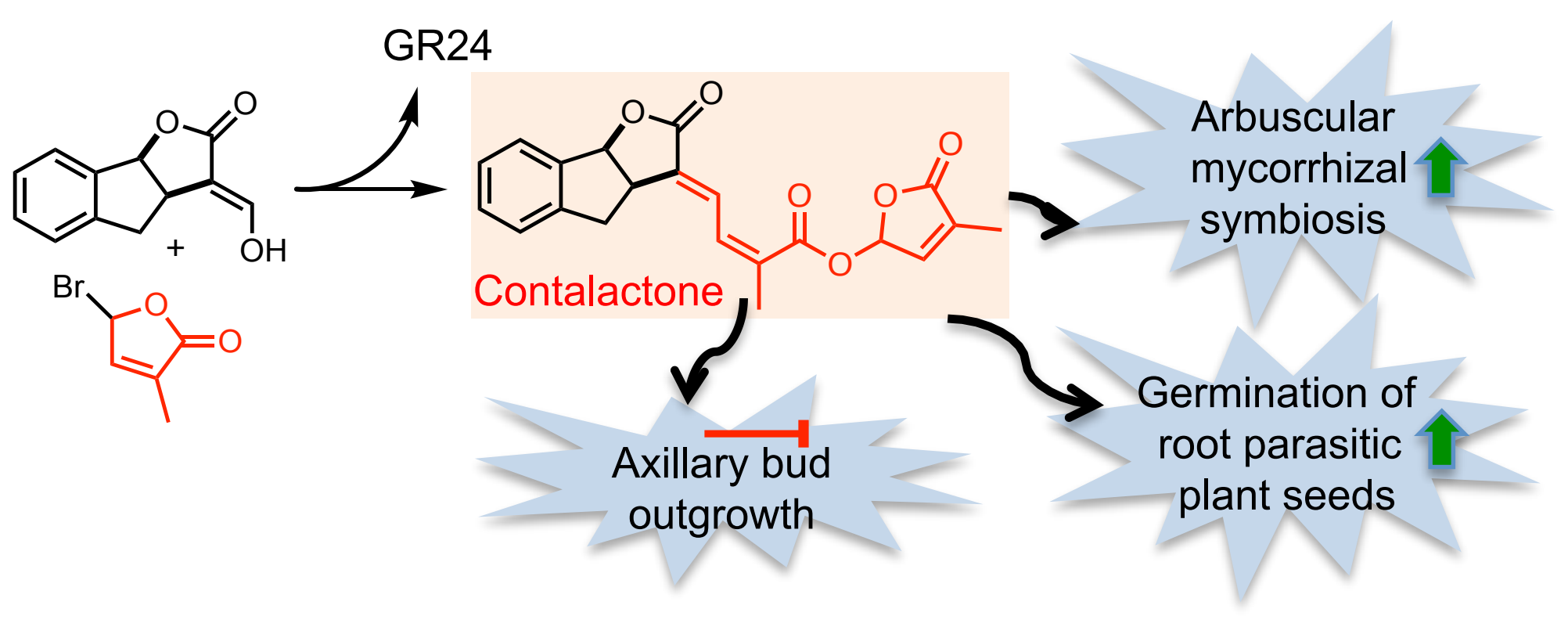
GR24
O
O
+
OH
Br
O
O
O
O
O
O
O
Contalactone
Arbuscular
mycorrhizal
symbiosis
Axillary bud
outgrowth
Germination of
root parasitic
plant seeds

Contalactone, a Contaminant Formed During Chemical Synthesis of the Strigolactone Reference GR24 is also a Strigolactone Mimic

Alexandre de Saint Germain,[1*] Pascal Retailleau,[2] Stéphanie Norsikian,[2] Vincent Servajean,[2] Franck Pelissier,[2] Vincent Steinmetz,[2] Jean-Paul Pillot,[1] Soizic Rochange,[3] Jean-Bernard Pouvreau,[4] and François-Didier Boyer[1,2*]

[1] Institut Jean-Pierre Bourgin, INRA, AgroParisTech, CNRS, Université Paris-Saclay, 78000, Versailles, France

[2] Institut de Chimie des Substances Naturelles, CNRS UPR2301, Univ. Paris-Sud, Université Paris-Saclay, 1 av. de la Terrasse, F-91198 Gif-sur-Yvette, France

[3] Laboratoire de Recherche en Sciences Végétales, Université de Toulouse, CNRS, UPS, 24 chemin de Borde Rouge, Auzeville, BP42617, 31326, Castanet Tolosan, France

[4] Université de Nantes, Laboratoire de Biologie et Pathologie Végétales, LBPV, EA 1157, F-44000 Nantes, France

*Correspondence to: François-Didier Boyer, Alexandre de Saint Germain E-mail: francois-didier.boyer@cnrs.fr, Alexandre.De-Saint-Germain@inra.fr ;

Corresponding author (Tel +33 1 69 82 30 17 ; Fax +33 1 69 07 72 47)

Title

Contalactone, a Contaminant Formed During Chemical Synthesis of the Strigolactone Reference GR24 is also a Strigolactone Mimic

Abstract. Strigolactone (SL) plant hormones control plant architecture and are key players in both symbiotic and parasitic interactions. GR24, a synthetic SL analog, is the worldwide reference compound used in all bioassays for investigating the role of SLs in plant development and in rhizospheric interactions. In 2012, the first characterization of the SL receptor reported the detection of an unknown compound after incubation of GR24 samples with the SL receptor. We reveal here the origin of this compound, which comes from the formation of a by-product during GR24 chemical synthesis. We present the identification of this by-product, named contalactone. A proposed chemical pathway for its formation is provided as well as an evaluation of its bioactivity on pea, *Arabidopsis*, root parasitic plant seeds and AM fungi, characterizing it as a SL mimic.

Keywords

Pisum sativum; Arabidopsis thaliana; Medicago truncatula; Root parasitic plants*; Rhizophagus irregularis;* Plant hormone*;* Structural determination*;* Strigolactone mimics*;* α/β-hydrolase

1. Introduction

Since 1966, it is known that Strigolactones (SLs), carotenoid-derived terpenoid lactones, exuded in the soil by host plant roots at picomolar doses, induce seed germination of *Striga* and *Orobanche* parasitic weeds (Cook et al., 1966; Xie et al., 2010). SLs are also involved in the establishment of symbiotic interactions between Arbuscular Mycorrhizal (AM) fungi and over 80% of plant species (Akiyama et al., 2005; Besserer et al., 2006). In 2008, SLs were identified as a new class of plant hormones involved in the control of shoot branching (Gomez-Roldan et al., 2008; Umehara et al., 2008) and many other traits (Lopez-Obando et al., 2015). Since then, the number of studies and publications on SLs increased dramatically (Waters et al., 2017). To date, more than 30 natural SLs have been isolated from plants. The structural core of SLs is a tricyclic lactone (ABC part, canonical SLs) or a variety of

structures (non-canonical SLs) connected via an enol ether bridge to an invariant α,β-unsaturated furanone moiety (D ring) (Yoneyama et al., 2018).

The great importance of SLs in plant chemical biology, their extremely low bio-availability, their sensitivity to hydrolysis and the difficulties to obtain natural SLs by organic synthesis due to long multi-step syntheses (Bromhead and McErlean, 2017; Yasui et al., 2017) prompted chemists to develop SL analogs. Numerous SL analogs and mimics easily accessible in sizeable quantities, more stable and with similar bioactivity as natural SLs have been described (Takahashi and Asami, 2018; Zwanenburg et al., 2016b).

GR24, a synthetic aromatic SL analog, invented by **G**erald **R**osebery, was initially developed for its high activity as parasitic seed germination stimulant and its increased stability compared to natural SLs (Akiyama et al., 2010; Boyer et al., 2012; Johnson et al., 1981). (±)-GR24 is accessible by organic synthesis on a multigram scale in six chemical steps from commercially available compounds (Mangnus et al., 1992). Today, GR24 is the reference compound in all bioassays investigating the role of SLs in plant development and in rhizospheric interactions.

Rapid progress in the understanding of SL perception has been made with the identification of the SL receptor (D14) in vascular plants as a member of the α/β-hydrolase superfamily containing the Ser, His and Asp catalytic triad located in a hydrophobic active site (Hamiaux et al., 2012). Biochemical analyses of D14 recombinant proteins from different species (*Arabidopsis*, pea, petunia, rice*)* showed that these receptors catalyze the hydrolysis of GR24 into 5-hydroxy-3-methylbutenolide (D-OH) and ABC=CHOH tricycle. The importance of the hydrolysis to trigger the signaling pathway is still debating (de Saint Germain et al., 2016; Seto et al., 2019; Shabek et al., 2018; Yao et al., 2016). We characterized the hydrolytic activity of the pea SL receptor (PsD14/RMS3) by incubating (±)-GR24 with RMS3. We observed products corresponding to the ABC=CHOH tricycle, and an unexpected compound of 270 $g.mol^{-1}$ (hereafter referred to as P270) already detected by other groups (Hamiaux et al., 2012; Zhao et al., 2015). The hypothesis of a second position of hydrolysis of GR24 was proposed. We rather suspected that it resulted from hydrolysis of a by-product of the GR24 synthesis. Here we present the identification of P270 and its precursor, that we named contalactone (for **conta**minant **lactone** of GR24), their bioactivity on different target organisms and a proposed chemical pathway for their formation.

2. Results and discussion

2.1 Detection and chemical characterization of (±)-contalactone, a contaminant of GR24

In order to determine the structure of the P270 compound, purified RMS3 protein was incubated with (±)-GR24 synthesized in our lab according to a known procedure (Mangnus et al., 1992) and purified by flash chromatography on silica gel (de Saint Germain et al., 2016) (Supp. Fig. 1) along with samples of (±)-GR24 from three commercial suppliers (Supp. Fig. 2-4). The analysis of products by UPLC-MS analysis led in all cases to the detection of both ABC=CHOH tricycle and P270 (Supp. Fig. 1-4). Compound P270 was also detected after incubation of (±)-GR24 samples at pH 9.4 for several hours at room temperature suggesting its formation by hydrolysis in alkaline aqueous condition as for ABC=CHOH tricycle (Fig. 1A). The maximum of UV absorbance of P270 is at 280 nm different from ABC=CHOH and GR24 which makes it easier to detect this compound at this wavelength. We also observed the product P270 from (±)-2'-*epi*-GR24 samples after enzymatic (de Saint Germain et al., 2016) or chemical treatment. From this observation, we then undertook purification of P270 starting from a 400-mg (±)-2'-*epi*-GR24 sample hydrolyzed under alkaline conditions to obtain enough amount of the pure compound P270 for complete characterization (Supp. Fig. 5). Its HR-ESI-TOF-MS afforded an ion at *m/z* 269.0811 $[M–H]^-$ calculated for $C_{16}H_{13}O_4$, *m/z* 269.0814 (Supp. Fig. 6). ^1H and ^{13}C NMR spectroscopic data established unambiguously the chemical structure of P270 (Fig. 1B, Supp. Fig. 7). P270 shows an ABC tricycle with a carbon chain of 5 carbons ended by a carboxylic function that totally differs from the D ring of SLs.

Due to its chemical structure and because P270 appeared after hydrolysis of (±)-GR24, we hypothesized that it derived from the *C*-alkylated precursor represented in Fig. 1B, and called this compound contalactone. We established P270 formation from contalactone, itself synthesized by *C*-alkylation of ABC=CHOH at very low level (<3%) (Fig. 1B) as described below. Zwanenburg and coll. (Thuring et al., 1997) have already reported the possibility to form, during the synthesis of SL analogs, substantial amounts of *C*-alkylated derivatives depending on the substrates and conditions. After several attempts involving modifications of base, solvent and temperature (Supp. Table 1), we were able to synthesize a significant amount of (±)-contalactone, isolated by careful purification with preparative HPLC. (±)-Contalactone was unambiguously identified by X-ray, mass and NMR analyses (Supp. Fig. 8-

11) as a mixture (1:1) of two diastereomers (contalactoneF1 and contalactoneF2) (Fig. 2, Supp. Fig. 12, Supp. Table 2). (±)-Contalactone is an ABC tricycle lactone with a five carbons chain, connected via an ester bridge to the D ring. As expected if the precursor of P270 was a contaminant, we did not detect P270 in assays performed with (±)-GR24 purified by preparative HPLC as reported (de Saint Germain et al., 2016)) and see Supp. Fig. 13. Contalactone was initially difficult to detect in GR24 or 2'-*epi*-GR24 samples due to its low abundance (2-4%) and its close retention time relative to that of GR24 isomers in UPLC/HPLC analyses that mask its presence (de Saint Germain et al., 2016; Hamiaux et al., 2012; Zhao et al., 2015).

A pathway for contalactone formation is proposed involving the *C*-alkylation of ABC=CHOH with D-Br, the formation of carboxylate either by a direct loss of formic acid, or by a loss of CO_2 via a base-induced redox reaction to an intermediate carboxylate, and a subsequent esterification with a second D-Br (Supp. Fig. 14).

2.2 (±)-Contalactone is hydrolyzed by RMS3, AtD14 and AtKAI2

To confirm that acid P270 can be formed from (±)-contalactone by RMS3 with a mechanism similar to GR24 cleavage we performed enzymatic assays by incubation of the purified contaclactone with the pea and *Arabidopsis* SL receptor RMS3 and AtD14. Both RMS3 and AtD14 recombinant proteins hydrolyze (±)-contalactone efficiently (Fig. 2A). In the absence of RMS3 or in the presence of the catalytic triad mutant protein $RMS3^{S96A}$ unable to hydrolyze SLs (de Saint Germain et al., 2016), no P270 was formed (Supp. Fig. 15A). We can unambiguously conclude that the P270 is coming from the hydrolysis of contalactone by SL receptor. Moreover, the hydrolysis of (±)-contalactone in basic aqueous medium led to the formation of (±)-P270 (Supp. Fig. 15B). Surprisingly, the recombinant AtKAI2 protein (also known as AtHTL), a paralog of AtD14 involved in hypocotyl development (Waters et al., 2012), hydrolyzed (±)-contalactone more efficiently than (±)-GR24 (Fig. 2A). The chemical hydrolysis of (±)-contalactone in comparison with (±)-GR24 was evaluated in a mixture ethanol/water at pH 6.8, corresponding to that used for enzymatic hydrolysis. (±)-Contalactone was less stable than (±)-GR24 (contalactone $t_{1/2} \approx 40$ h, GR24 $t_{1/2} \approx 290$ h) (Fig. 2B). We can hypothesize that contalactone may be an efficient substrate of AtKAI2 as GR24 in connection to its high sensitivity to hydrolysis as demonstrated by its low stability in aqueous solution.

2.3 (±)-Contalactone is able to inhibit branching in pea and interacts with the SL receptor RMS3

The discovery of the contaminant in GR24 samples raises the question of its bioactivity. The biological activities of (±)-contalactone and (±)-P270 were evaluated using a pea branching assay with the highly branched SL-deficient *rms1-10* mutant (de Saint Germain et al., 2016). (±)-Contalactone showed activity at a concentration of 5 µM but was found to be significantly less active than (±)-GR24 since contalactone was not active at 500 nM or below (Fig. 3, Supp. Table 3). Moreover, (±)-contalactone was inactive on the branching of the pea *rms3-5* perception mutant (Fig. 3, Supp. Table 4). No bioactivity of the contalactone hydrolysis product, (±)-P270, was detected even at high concentration (10 µM) as for ABC=CHOH tricycle (Supp. Table 3). These results suggest that (±)-contalactone, as GR24, is a specific bioactive SL mimic and inhibits bud outgrowth via the RMS3 receptor, and not because of toxicity. In order to validate that (±)-contalactone is perceived by the pea SL receptor RMS3, we performed differential scanning fluorimetry (DSF) and revealed a shift in RMS3 melting temperature in the presence of (±)-contalactone, corresponding to a protein destabilization as for the SL bioactive analogs (see (±)-GR24). No interaction between the RMS3 protein and (±)-P270 was observed (Fig. 4). We estimated the binding affinity of (±)-contalactone towards RMS3 by intrinsic fluorescence and found a K_D value of 64.12 ± 16.09 µM slightly lower than for (±)-GR24 (K_D = 14.66 ± 9.63 µM) (Fig. 4B-C). The lower affinity of (±)-contalactone for RMS3 is in agreement with the lower bioactivity of these compounds on pea branching inhibition.

2.4 (±)-Contalactone represses hypocotyl elongation in Arabidopsis via AtD14 and AtKAI2

We also tested the bioactivity of (±)-contalactone and (±)-P270 on *Arabidopsis* hypocotyl elongation with SL biosynthesis (*max3-11*) and perception (*Atd14-1*, *htl-3*, *max2-1*) mutants. In *Arabidopsis*, (±)-GR24 inhibits hypocotyl growth via AtD14 and AtKAI2 (AtHTL) (Waters et al., 2017; Waters et al., 2012). Like (±)-GR24, (±)-contalactone significantly suppressed hypocotyl elongation in wild-type plant and also in *max3-11*, *Atd14-1* and *htl-3* mutants seedlings, but not in the *max2-1* mutant. These results confirm that (±)-contalactone can mimic the GR24 effect not only on branching but also on hypocotyl elongation. These results show that (±)-contalactone repressed hypocotyl elongation via AtMAX2, and redundantly via AtD14 and AtKAI2, as already demonstrated for GR24 (Nelson et al., 2011).

This suggests that AtKAI2 can perceive (±)-contalactone. However, (±)-P270 does not repress hypocotyl elongation in wild-type, *max3-11* or *Atd14-1* mutant seedlings. We observed a slight inhibition of hypocotyl elongation in *htl-3* and especially in *max2-1* mutant probably due to a toxic effect (Fig. 5).

2.5 (±)-Contalactone is a potent germination stimulant of various root parasitic plants

Root parasitic seed germination is the most sensitive assay to evaluate the SL activity of compounds and also to detect the presence of natural SLs in samples. The germination stimulant (GS) activities of (±)-contalactone on *Orobanche cumana, Phelipanche ramosa* and *Striga hermonthica* parasitic plant seeds were determined by measuring the maximum of GS activity as well as half maximal effective concentrations (EC_{50}). GS activities of (±)-contalactone reached the maxima induced by GR24 isomers or other GSs (an isothiocyanate (2-PEITC) (Auger et al., 2012) or the terpenoid dehydrocostus lactone (DCL) (Joel et al., 2011)) for *P. ramosa* and *O. cumana*, respectively (Fig. 6A), except with *S. hermonthica* (54%). The lowest EC_{50} was observed with (+)-GR24 for all tested parasitic plant species. In *P. ramosa*, the EC_{50} of (±)-contalactone was intermediate compared to (+)-GR24 (about 100-fold less active), similar to (−)-GR24 or (+)-2'-*epi*-GR24, but better or similar to 2-PEITC depending on the genetic population (Fig. 6B, Supp. Fig. 16). For *S. hermonthica* seeds, the (±)-contalactone activity was also moderate compared to (+)-GR24 (about 100-fold less active) but similar to the three other GR24 isomers. For *O. cumana,* (±)-contalactone exhibited very high EC_{50} in comparison with (+)-GR24 and DCL (1,000,000 and 10,000-fold less activity, respectively) but possessed similar activity to (−)- and (+)-2'-*epi*-GR24. Additionally, no significant difference of germination activity was found between the two diastereomers of (±)-contalactone except for *S. hermonthica* at 10^{-7}-10^{-8} M (Supp. Fig. 17). To summarize, (±)-contalactone is an efficient GS compared with many SL analogs and mimics described in the literature (Takahashi and Asami, 2018; Zwanenburg et al., 2016b).

2.6 (±)-Contalactone induces the colonization of AM fungi in Medicago truncatula

SLs are known to increase hyphal branching of AM fungi (Akiyama et al., 2005; Besserer et al., 2006) and this biological response can be measured *in vitro* to characterize the activity of SLs, SL analogs and mimics (Akiyama et al., 2010; Mori et al., 2016). However, a causal link between this branching response and symbiosis has not been established. Here, we used a

different assay in which SL-deficient mutants of *M. truncatula* are inoculated with the AM fungus *Rhizophagus irregularis*. The roots of these mutants are hardly colonized, likely due to deficient stimulation of the AM fungus. Treatment with (±)-GR24 can increase the number of root infection units (Fig. 7), and thus this test can be used as a bioassay to assess the effect of SL mimics on AM symbiotic ability. (±)-Contalactone applied at 100 nM was able to enhance significantly the level of root colonization by *R. irregularis*, although the activity was slightly lower than that of (±)-GR24 (Fig. 7). Thus, in addition to the effects on plants reported above, (±)-contalactone also shows significant bioactivity on symbiotic fungi.

3. Concluding remarks

To summarize, our results show that a contaminant, that we named contalactone, can be present in GR24 samples. Contalactone is obtained in the last synthesis step of GR24. Because the last step of chemical synthesis process of all SLs and analogs is similar to that of GR24 (Bromhead and McErlean, 2017; Yasui et al., 2017; Zwanenburg et al., 2016a), we can speculate that all SLs and analogs could be contaminated by this type of compound. Contalactone is bioactive as plant hormone, as inducer of colonization of plants by AM fungi and GS for root parasitic plant seeds. Contalactone can be identified as a novel SL mimic structurally similar to previously described aroyloxy butenolides which have been characterized as GS for *S. hermonthica, O. cernua* and *P. ramosa* seeds. However these aroyloxy butenolides showed lower bioactivity (Zwanenburg and Mwakaboko, 2011; Zwanenburg et al., 2013; Zwanenburg et al., 2016b). Contalactone is rapidly transformed by the SL receptor into a non-bioactive compound P270. Because contalactone is bioactive, it is important to synthesize GR24 by a method producing low amounts of contalactone (Entry 1, Supp. Table 1) and to remove it from GR24 samples by careful purification (HPLC). Since contalactone is hydrolyzed faster than GR24, we can also suggest to purify GR24 sample by a final step of alkaline hydrolyze to eliminate residual contalactone. The quality of GR24 samples can also be checked by carrying out microscale hydrolysis in a basic aqueous medium that makes it easier to detect P270 than contalactone in the starting samples. The purity of chemicals used for biology experiments is essential and deviations to this rule can easily lead to misinterpretations of biochemistry results and biological effects. An alternative to GR24 could be the use of SL mimics (Takahashi and Asami, 2018) for which it is not possible to form contalactone-like compounds during coupling to incorporate the D ring and

for which an identical mode of action was demonstrated, e.g. GC242 (de Saint Germain et al., 2016).

4. Experimental

4.1 General chemical procedures

All non-aqueous reactions were run under an inert atmosphere (argon), by using standard techniques for manipulating air-sensitive compounds. All glassware was stored in the oven and/or was flame-dried prior to use. Anhydrous solvents were obtained by filtration through drying columns. Analytical thin-layer chromatographies (TLC) were performed on plates precoated with silica gel layers. Compounds were visualized by one or more of the following methods: (1) illumination with a short wavelength UV lamp (i.e., $\lambda = 254$ nm), (2) spray with a 3.5% (w/v) phosphomolybdic acid solution in absolute ethanol. Flash column chromatography was performed using 40-63 mesh silica. Nuclear magnetic resonance spectra (^{1}H ; ^{13}C NMR) were recorded respectively at [500; 125] MHz on a Bruker DPX 500 spectrometer. For the ^{1}H spectra, data are reported as follows: chemical shift, multiplicity (s = singlet, d = doublet, t = triplet, q = quartet, m = multiplet, bs = broad singulet, coupling constant in Hz and integration. IR spectra are reported in reciprocal centimeters (cm^{-1}). Buffers and aqueous mobile-phases for HPLC were prepared using water purified with a Milli-Q system. Mass spectra (MS) and high-resolution mass spectra (HRMS) were determined by electrospray ionization (ESI) coupled to a time-of-flight analyser (Waters LCT Premier XE).

4.2 Preparation of GR24 isomers

(±)-2'-*epi*-GR24 and (±)-GR24 were prepared according to described procedures (Mangnus et al., 1992). (±)-GR24 suppliers used in this manuscript are Chiralix™, Strigolab™ and OlChemIm™. (+)-GR24, (−)-GR24, (+)-2'-*epi*-GR24, (−)-2'-*epi*-GR24 were separated from (±)-2'-*epi*-GR24 and (±)-GR24 by chiral supercritical fluid chromatography as described in (de Saint Germain et al., 2016). Dehydrocostus lactone (DCL) and 2-phenethyl isothiocyanate (2-PEITC) are commercially available. (±)-GR24 can be purified by semi-preparative HPLC. Semi-preparative HPLC was performed using an Interchim puriFlash® 4250 instrument, combined with a fraction collector with integrated ELSD, a PDA and a Phenomenex Luna

C_{18}, 250 × 21.2 mm, 5 µm column (H_2O/CH_3CN : 6 /4) or Interchim Uptisphere Strategy SI, 250 × 21.2 mm, 5 µm column (Heptane/EtOAc : 1 /1).

4.3 Preparation and isolation of (±)-contalactone

To solid K_2CO_3 (1.851 g, 13.4 mmol) dried under reduced pressure was added at room temperature under argon anhydrous acetone (27 mL). After 10 min, a mixture of ABC=CHOH (1.354 g, 6.7 mmol) and D-Br (1.778 g, 10.5 mmol) in anhydrous acetone (67 mL) was added dropwise to the preceding solution. The resulting reaction mixture was stirred for 20 h at room temperature under argon and acetone evaporated under reduced pressure. The residue was diluted in EtOAc and filtered. This reaction was performed at this scale several times to obtain a crude product (38.39 g) which contains a mixture of (±)-GR24, (±)-2'-*epi*-GR24 and (±)-contalactone (45.5:45.5:9) (ratio determined by ^{1}H NMR). The crude mixture was purified by medium pressure chromatography on silica gel and HPLC (Interchim Uptisphere Strategy SI, 250 × 21.2 mm, 5 µm column) (Heptane/EtOAc : 1 /1) to furnish pure (±)-GR24, (±)-2'-*epi*-GR24 and (±)-contalactone. However, the two diastereomers of (±)-contalactone can be separated by HPLC using a *Hypercarb* porous graphitic carbon column (100 × 4.6 mm, 5 µm) (MeOH/iPrOH 1/1, Formic acid 0.1%, 2 mL/min) to furnish contalactoneF1 (1.5 mg) (>99%) and contalactoneF2 (0.7 mg) (>95%) after 30 injections and evaporation under reduced pressure.

(±)-Contalactone: mixture of two diastereomers (1:1): M.p. 185.0-209.4 °C. ^{1}H NMR (300 MHz, $CDCl_3$) δ: 7.92 (d, *J* = 12.0 Hz, 1H), 7.55 (d, *J* = 7.2 Hz, 1H), 7.40-7.24 (m, 3H), 7.02-6.95 (m, 2H), 6.72 (d, *J* = 12.0 Hz, 1H), 6.00 (d, *J* = 8.0 Hz, 1H), 4.11-4.02 (m, 1H), 3.69 (dd, *J* = 16.5 Hz, *J* = 10.0 Hz, 1H), 2.97 (dd, *J* = 16.5 Hz, *J* = 3.0 Hz, 1H), 2.18 (s, 3H), 2.03 (s, 3H). ^{13}C NMR (75.5 MHz, $CDCl_3$) δ: 171.1 (Cq), 170.1 (Cq), 164.6 (Cq), 143.1 (Cq), 142.4 (Cq), 142.0 (CH), 138.7 (Cq), 136.6 (Cq), 134.9 (Cq), 134.8 (CH), 134.7 (CH), 134.49 (Cq), 134.46 (Cq), 131.7 (CH), 130.5 (CH), 127.9 (CH), 126.7 (CH), 125.2 (CH), 97.1 (CH), 93.1 (CH), 85.9 (CH), 39.82 (CH_2), 39.77 (CH_2), 21.6 (CH_3), 10.90 (CH_3). IR ν (film, cm^{-1}): 2952, 2924, 2853 (CH), 1780 and 1748 (C=O). HRMS (ESI): Calculated for $C_{21}H_{18}O_6Na$ [M + Na^+]: 389.1001. Found: 389.0996.

4.4 Preparation and isolation of (±)-P270

To a sample of (±)-2'-*epi*-GR24 purified by flash chromatography on silica gel (Mangnus et al., 1992) (400 mg, 1.34 mmol) in THF (10 mL) was added a *phosphate buffered saline (*PBS buffer, pH 6.8) solution (10 mL) and dropwise a aqueous solution of KOH (1 M) until pH 9.5. The resultant solution was stirred for 10 h at room temperature and extracted with CH_2Cl_2 (3 × 20 mL). The combined organic layer was dried (Na_2SO_4), filtered and evaporated under reduced pressure to afford 370 mg of (±)-2'-*epi*-GR24 containing no P270. The aqueous phase was acidified until pH 2 and extracted with CH_2Cl_2 (3 × 20 mL). The combined organic layers were dried (Na_2SO_4), filtered and evaporated under reduced pressure to afford 79 mg of crude product containing a small amount of (±)-2'-*epi*-GR24, ABC=CHOH and P270. P270 was purified by semi-preparative HPLC which was performed using an Interchim puriFlash® 4250 instrument, combined with a fraction collector with integrated ELSD, a PDA and a Phenomenex Luna C_{18}, 250 × 21.2 mm, 5 µm column (0.1% formic acid in CH_3CN (solvent B) and 0.1% formic acid in water (solvent A). A/B (7/3) isocratic 5 min then linear gradient to A/B (2/8) in 20 min at a flow rate of 1 mL/min. P270 was obtained as a white solid after lyophilisation (5 mg, 0.018 mmol, 1.4%).

P270: ^{1}H NMR (500 MHz, $CDCl_3$) δ: 7.82 (dd, *J* = 12.0 Hz, *J* = 10.2 Hz, 1H), 7.53 (d, *J* = 7.2 Hz, 1H), 7.37 (dd, *J* = 8.0 Hz, *J* = 7.2 Hz, 1H), 7.30-7.27 (m, 2H), 6.71 (d, *J* = 12.0 Hz, 1H), 5.96 (d, *J* = 7.6 Hz, 1H), 4.15-4.09 (m, 1H), 3.69 (dd, *J* = 17.0 Hz, *J* = 10.0 Hz, 1H), 2.97 (dd, *J* = 17.0 Hz, *J* = 2.4 Hz, 1H), 2.11 (s, 3H). ^{13}C NMR (125 MHz, $CDCl_3$) δ: 172.2 (Cq), 169.3 (Cq), 149.1 (Cq), 147.9 (Cq), 144.4 (Cq), 140.2 (Cq), 133.0 (CH), 132.0 (CH), 131.1 (CH), 128.4 (CH), 127.3 (CH), 126.3 (CH), 86.9 (CH), 40.6 (CH), 40.3 (CH_2), 21.9 (CH_3). IR ν (film, cm^{-1}): 3600-2400 (br, CO<u>OH</u>), 2935, 1747 (C=O), 1638. HRMS (ESI): Calculated for $C_{16}H_{13}O_4$ [M – H]: 269.0814. Found: 269.0811.

4.5 Crystallographic data collection, structure determination and refinement

X-ray structure determination for contalactone (FDB2980F1**)** was carried out at low temperature (173K) using a RIGAKU XtaLabPro diffractometer equipped with a Mo microfocus sealed tube generator coupled to a double-bounce confocal Max-Flux® multilayer optic and a HPAD PILATUS3 R 200K detector. Data collection and processing were performed with the CrysalisPro software (Rigaku, 2015). The structure was solved by intrinsic phasing methods (SHELXT program) (Sheldrick, 2015b) then refined by full-matrix least-squares methods (SHELXL-2018/3 program) (Sheldrick, 2015a). Non-hydrogen atoms

improved by anisotropic refinement, whereas H atoms bonded to C atoms were included in the structure at idealized positions, and refined using a riding model, with U_{iso}(H) = 1.2U_{eq}(C) and C—H = 0.95-0.99-1.00 Å for aromatic, methylene, and methine H atoms, respectively, whereas for methyl groups, U_{iso}(H) = 1.5U_{eq}(C) and C—H = 0.98 Å. A second polymorph coexists in the crystallization medium, more massive than the elongated platelet, and was characterized at 173 K as a triclinic crystal. The diastereomer that was determined subsequently differs from the monoclinic one at the level of the lactone tail (torsion angles C9' – O14' -C2'- O1' 110.8° (triclinic) *vs* -77.6° (monoclinic)) (see the model overlay in the Figure 1C). Crystallographic data (including structure factors) for the structures, FDB2980F1 dia1 and FDB2980F1 dia2, reported in this paper have been deposited with the Cambridge Crystallographic Data Centre as supplementary publication no. CCDC-1870390-1870391 respectively. Copies of the data can be obtained free of charge on application to CCDC, 12 Union Road, Cambridge CB21EZ, [fax: (internat.) + 44 1223/336-033; e-mail: deposit@ccdc.cam.ac.uk].

4.6 Plant material and growth conditions

Pea (*Pisum sativum*) branching mutant plants used in this study were derived from various cultivars of pea after ethyl methanesulfonate (EMS) mutagenesis and were described previously (Rameau et al., 1997). The *rms1-10* (M3T-884) and *rms3-5* (M2T-32) mutants were obtained from the dwarf cv Térèse. Plants were grown in a greenhouse under long days as described in (Braun et al., 2012).

All *A. thaliana* plants used in this study originated from the Columbia (Col-0) ecotype background and have been described previously: *Atd14-1, max2-1* (Stirnberg et al., 2002) and *htl-3* (Toh et al., 2014). The *max2-1* mutant was provided by P. Brewer (University of Queensland,), *Atd14-1* mutant was provided by M. Waters (University of Western Australia), and *htl-3* was provided by P. McCourt (University of Toronto). Plants were grown in a growth room under long-day conditions (16 h light/8 h dark). Seeds were sown onto solid agar (0.8%, w/v) in Petri dishes and stratified at 4 °C in darkness for 48 h, then transferred to white light (120 µmol m^{-2} s^{-1}). Seedlings were grown for 5 d or 6 d and were transplanted to individual plastic pots (0.2 L) with a 1:1:1 vermiculite:perlite:peat mixture, and grown in a glasshouse under natural light, until they were 48 d old. The greenhouse experiments were carried out in the spring, under long photoperiods (15–16 h per day); daily temperatures

fluctuated between 18 °C and 25 °C. Peak levels of PAR were between 700 and 1,000 µmol m^{-2} s^{-1}. Plants were watered twice a week with tap water.

Four batches of parasitic plant seeds were used in this study. A population of seeds of *Phelipanche ramosa (L.)* Pomel associated to genetic group 1 (*P. ramosa* 1) was collected from Saint Martin-de-Fraigneau, France, on broomrape parasitizing winter oilseed rape (*Brassica napus* L.) in 2015 and seeds of *P. ramosa* from genetic subclade 2a (*P. ramosa* 2a) from Saint Martin-de-Bossenay, France, on broomrape developed on hemp (*Cannabis sativa* L.) in 2012 (Stojanova et al., 2019). *Orobanche cumana* Wallr. seeds were harvested on broomrape parasitizing sunflower (*Helianthus annus* L.; Longeville-sur-mer, France, 2017). Seeds of *Striga hermonthica* (Delile) Benth. (Sudan, 2007) were provided by Lukas Spichal (The Czech Republic). Seeds were surface sterilized and conditioned according to (Pouvreau et al., 2013) (dark condition; 21 °C for *P. ramosa* and *O. cumana;* 30 °C for *S. hermonthica*).

4.7 Pea shoot branching assay

The compounds to be tested were applied directly to the axillary bud with a micropipette as 10 µL of a solution containing 0.1% DMSO with 2% polyethylene glycol 1450, 50% ethanol and 0.4% DMSO (Boyer et al., 2012). The control-0 is the treatment with 0.1% DMSO without compound. 24 plants were sown per treatment in trays (2 repetitions of 12 plants). The treatment was generally done 10 days after sowing, on the axillary bud at node 3. The branches at nodes 1 to 2 were removed to encourage the outgrowth of axillary buds at nodes above. Nodes were numbered acropetally from the first scale leaf as node 1 and cotyledonary node as node 0. Bud growth at node 3 was measured with digital callipers 8 to 10 days after treatment. Plants with damaged main shoot apex or showing a dead white treated-bud were discarded from the analysis. The SL-deficient *rms1-10* pea mutant was used for all experiments.

4.8 Arabidopsis hypocotyl elongation assays

Arabidopsis seeds were sterilized with 95% ethanol for 10 min, and were plated on half Linsmaier and Skoog (LS) media (Caisson laboratories) containing 0.8% agar, supplemented with indicated concentrations of (±)-contalactone and (±)-GR24 (stock 1000 × in DMSO) or with DMSO (control). Seeds were stratified at 4 °C (2 days in dark) then transferred in growth chamber at 22 °C, under 20-30 µE /m^2/sec of white light in long day conditions (16 hr light/ 8

hr dark). Plates were photographed and hypocotyl lengths were quantified using ImageJ (http://imagej.nih.gov/ij/).

4.9 Germination stimulation activity assay on root parasitic plant seeds

Germination Stimulant activity (GS) of chemicals on seeds of parasitic plants were determined using a method described previously (Pouvreau et al., 2013). Chemicals were suspended in DMSO at 10 mmol L^{-1}, then diluted with water at 1 mmol L^{-1} (water/DMSO; v/v; 9/1). Dilutions of 1×10^{-5} mol L^{-1} to 1×10^{-12} mol L^{-1} are then performed in water/DMSO (v/v; 9/1). For each compound, a range of concentrations from 10^{-13} to 10^{-6} mol L^{-1} (water/DMSO; 99/1) were applied to conditioned parasitic seeds. DMSO 1% was used as negative control (seed germination < 1%) and (±)-GR24 at a concentration of 1 µmol L^{-1} was used as a positive control and induced 72-87 % of seed germination for *P. ramosa* 1, 80–90% for *P. ramosa* 2a, 85-95 % for *O. cumana* and 50-65% for *S. hermonthica*. To avoid variations related to sterilization events percentages of germination are reported as a ratio relative to the positive control ((±)-GR24, 1 µmol L^{-1}) included in each germination assay. Each dilution and germination assay was repeated at least three times. For each compound tested, dose-response curves (GS = f(c), Germination Stimulant activity relative to (±)-GR24 1 µmol L^{-1} ; c : concentration (mol. L^{-1}), half maximal effective concentration (EC_{50}), and maximum of germination stimulant activity were determined using a Four Parameter Logistic Curve computed with SigmaPlot® 10.0.

4.10 Assay of activity on Rhizophagus irregularis

SL-deficient *ccd8-1* mutants of *Medicago truncatula* (Lauressergues et al., 2015) were placed in 50-mL pierced Falcon tubes containing OilDri substrate inoculated with 150 spores of *R. irregularis*. 1000X concentrated solutions of SL analogs in acetone were added to the nutrient solution, to reach a final concentration of 10^{-7} M. Mock treatments (CTL0) were performed with the solvent alone. The number of infection points in the whole root system was recorded three weeks post-inoculation, allowing to assess the improved symbiotic ability of *R. irregularis* following treatment with SL analogs.

4.11 Expression and purification of proteins

Expression and purification of proteins RMS3, $RMS3^{S96A}$, $RMS3^{H247A}$, $RMS3^{D218A}$,

RMS3^{S96C} and AtKAI2 with cleavable GST tag were performed in accordance with (de Saint Germain et al., 2016).

4.12 Enzymatic degradation of (±)-contalactone and (±)-GR24, by purified RMS3 /AtKAI2 proteins

The ligand (10 µM) was incubated without and with purified RMS3/RMS3^{S96A}/AtKAI2 (5 µM) for 210 min at 25 ºC in PBS (0.1 mL, pH = 6.8) in presence of (±)-1-indanol (100 µM) as internal standard. The solutions were acidified to pH = 1 by addition of trifluoroacetic acid (2 µL) to quench the reaction and centrifugated (12 min, 12,000 tr/min). Thereafter the samples were subjected to RP-UPLC-MS analyses. The instrument used for all the analysis was an Ultra Performance Liquid Chromatography system equipped with a PDA and a Triple Quadrupole mass spectrometer Detector (Acquity UPLC-TQD, Waters, USA). RP-UPLC (HSS C_{18} column, 1.8 µm, 2.1 mm × 50 mm) with 0.1% formic acid in CH_3CN and 0.1% formic acid in water (aq. FA, 0.1%, v/v, pH 2.8) as eluents [5% CH_3CN, followed by linear gradient from 5 to 100% of CH_3CN (7 min)] at a flow rate of 0.6 mL/min. The detection was performed by PDA and using the TQD mass spectrometer operated in Electrospray ionization positive mode at 3.2 kV capillary voltage. The cone voltage and collision energy were optimized to maximize the signal and was respectively 20 V for cone voltage and 12 eV for collision energy and the collision gas was argon at a pressure maintained near of $4.5.10^{-3}$ mBar.

4.13 Hydrolysis of (±)-contalactone and (±)-GR24 in aqueous solution

(±)-GR24 and (±)-contalactone were tested for their chemical stability in an aqueous solution. Aqueous solutions of the compound to be tested (50 µg/mL) were incubated at 22 °C in the HPLC vials. The compounds were first dissolved in DMSO (2 mg/mL). Then, 25 µL of the previous solutions (GR24 and contalactone) were diluted to the final concentration with H_2O (750 µL) and EtOH (175 µL) and the solution adjusted to pH 6.8. Aqueous solutions of the compounds to be tested (50 µg/mL) were incubated at 22 °C in the HPLC vials. Indanol (Alfa Aesar, purity > 97.5% (GC)) (25 µL of a 1 mg/mL solution in DMSO) as internal standard was added to each solution. The time-course of degradation was monitored by UPLC analysis using the system described for the enzymatic degradation of GR24 and contalactone. Compounds eluted from the column were detected with a photodiode array detector. The

relative quantity of remaining (non degraded) product was determined by integration comparison with the internal standard.

4.14 Differential Scanning Fluorimetry (DSF)

DSF experiments were performed on a CFX384 Touch™ Real-Time PCR Detection System (Biorad) using excitation and emission wavelengths of 490 and 575 nm, respectively. Sypro Orange ($\lambda_{Ex}/\lambda_{Em}$: 490/610 nm; life technologie) was used as the reporter dye. Samples were heat-denatured using a linear 25 to 95°C gradient at a rate of 1.3 °C per minute after incubation of 25 °C for 30 min in the absence of light. The denaturation curve was obtained using CFX manager software. Final reaction mixtures were prepared in triplicate in 384-well white microplates, and each reaction was carried out in 20-µL scale in PB buffer pH 6.8 containing 10 µg protein, each concentration of SL derivatives (DMSO solution, final DMSO concentration was 4%), and 0.008 µL Sypro Orange. In the control reaction, DMSO was added instead of chemical solution.

4.15 Intrinsic tryptophan fluorescence assays and determination of the dissociation constant $K_{D.}$

Interaction of recombinant proteins with SL analogues was monitored by measuring the intrinsic tryptophan fluorescence using a Tecan Safire II Plate Reader in a 96-well format. In the assay, to a 50 µL ligand solution (10 different compound concentrations ranging from 0 to 800 µM were prepared from a 2 mM stock solution in 100% DMSO) in PBS buffer at pH 6.8, 50 µL of a solution of protein in same buffer was added simultaneously in a flat-bottomed, black 96-well plate using a Integra Viaflo 96 robot, to obtain 10 µM final protein concentration. The volume of DMSO in each well was identical. After 1 h incubation at 25 °C, fluorescence was measured. The excitation wavelength at 280 nm was used and an emission spectrum was recorded 5 times over the range of 300 to 400 nm and excitation and emission slit widths of 5 nm. The gain was set to 70, the number of flashes to 50, the flash frequency to 400 Hz, and the integration time to 2 ms.

To quantify the interaction between protein and ligand, the intensities of fluorescence at a fixed wavelength (333 nm) were measured. The degree of saturation (F_a) was determined by transforming the experimental data to the form:

$$F_a = \left| \frac{F_{obs} - F_0}{F_{max} - F_0} \right|$$

where F_0 is the fluorescence intensity in the absence of ligand, F_{obs} is the fluorescence intensity in the presence of non-saturating concentrations of ligand and F_{max} is the fluorescence intensity at saturation. For the K_d determination, the data were fitted by nonlinear regression with hyperbolic function using GraphPad Prism 5.0 software for overall one-site binding.

4.16 Statistical analyses

Because deviations from normality were observed for axillary bud length and hypocotyl length after SL treatment, the Kruskal–Wallis test was used to assess the significance of one treatment with one compound in comparison to treatment with another using R Commander version 1.7–3 (Fox, 2005). The Mann-Whitney test was also used.

Declaration of interest: none.

Acknowledgments

The authors thank Catherine Rameau for statistical analyses and Katie Martin for technical assistance. The authors thank also Catherine Rameau, Sandrine Bonhomme and Jean-Marie Beau for comments on the manuscript.

Appendix A. Supplementary data

Supplementary data to this article can be found online at https://doi.org/.

Supplementary Table 1. Conditions for the preparation of (±)-GR24 isomers and (±)-contalactone.

Supplementary Table 2. Experimental details for X-ray analysis of contalactone.

Supplementary Table 3. Bud outgrowth inhibition activity assay results for SL derivatives using *rms1-10* pea plants.

Supplementary Table 4. Bud outgrowth inhibition activity assay for (±)-contalactone and (±)-GR24 using *rms3-5* pea plants.

Supplementary Figure 1. Detection of the novel compound (P270) following enzymatic activity of the SL receptor from (±)-GR24 prepared according to (Mangnus et al., 1992).

Supplementary Figure 2. Detection of the novel compound (P270) following enzymatic activity of the SL receptor from (±)-GR24 purchased from supplier #1.

Supplementary Figure 3. Detection of the novel compound (P270) following enzymatic activity of the SL receptor from (±)-GR24 purchased from supplier #2.

Supplementary Figure 4. Detection of the novel compound (P270) following enzymatic activity of the SL receptor from (±)-GR24 purchased from supplier #3.

Supplementary Figure 5. Characterization of P270 by UPLC analysis.

Supplementary Figure 6. UPLC analysis and High Resolution Mass Spectrometry (HRMS) spectrum of P270 after purification.

Supplementary Figure 7. NMR spectra of P270.

Supplementary Figure 8. UPLC analysis of (±)-contalactone after preparative HPLC purification and UV spectrum of (±)-contalactone.

Supplementary Figure 9. MS spectrum and (±)-contalactone, and High Resolution Mass Spectrometry (HRMS) spectrum of (±)-contalactone.

Supplementary Figure 10. NMR spectra of of (±)-contalactone.

Supplementary Figure 11. An ORTEP plot of (±)-contalactone.

Supplementary Figure 12. HPLC separation of both diastereomers of (±)-contalactone.

Supplementary Figure 13. Elution profile of the enzymatic assay (RMS3) and the chemical assay (KOH) with (±)-GR24 obtained by careful purification with preparative HPLC.

Supplementary Figure 14. Proposed mechanism for the formation of (±)-contalactone (P270 precursor).

Supplementary Figure 15. Elution profile of the enzymatic assay (RMS3) and the chemical assay (KOH) with (±)-contalactone obtained by careful purification by preparative HPLC.

Supplementart Figure 16. Dose response activities and modeled curves for the Germination Stimulation (GS) activity on seeds of *P. ramosa, O. cumana* and *S. hermonthica* by (±)-contalactone. Comparison with GR24 isomers, dehydrocostus lactone (DCL) and 2-phenethyl isothiocyanate (2-PEITC).

Supplementary Figure 17. Germination Stimulation (GS) activity on seeds of *P. ramosa, O. cumana* and *S. hermonthica* by (±)-contalactoneF1, (±)-contalactoneF2 and (±)-contalactone.

Funding

We are grateful to the Agence Nationale de la Recherche (ANR-12-BSV6-004-01), and to the Stream COST Action FA1206 for financial support. This work has benefited from a French State grant (LabEx Saclay Plant Sciences-SPS, ANR-10-LABX-0040-SPS), managed by the French National Research Agency under an "Investments for the Future" program (ANR-11-IDEX-0003-02). A.d.S.G. has received the support of the EU in the framework of the Marie-Curie FP7 COFUND People Programme, through the award of an AgreenSkills/AgreenSkills+ fellowship. The work of S.R. was supported by the TULIP LabEx (ANR-10-LABX-41). The CHARM3AT Labex program (ANR-11-LABX-39) is also acknowledged for its support.

Figures and Legends

Figure 1. Detection of (±)-P270 and structure of (±)-P270 and (±)-contalactone. (**A**) Elution profile of the enzymatic assay of (±)-GR24 by RMS3, pH 6.8, (orange and red curves) or by alkaline hydrolysis at pH 9.4, (green curves) purified by flash chromatography on silica gel. UPLC with diode array detection (200-400 nm) shows the formation of ABC=CHOH (254 nm) and compound P270 (280 nm). (±)-Contalactone is not detected. (**B**) Synthetic scheme for the synthesis of (±)-GR24, (±)-2'-*epi*-GR24, (±)-contalactone and (±)-P270. (**C**) Model overlay of both diastereomers of (±)-contalactone obtained by X-ray analysis.

Figure 2. Hydrolysis assays with (±)-contalactone and (±)-GR24. (**A**) Enzymatic hydrolysis rate of (±)-contalactone and (±)-GR24 by RMS3, AtD14 and AtKAI2 proteins. UPLC-UV (260 nm) analysis shows the formation of the ABC=CHOH tricycle from (±)-GR24 and P270 from (±)-contalactone (confirmed by mass spectrometry analyses). The indicated percentage corresponds to the hydrolysis rate calculated from the remaining (±)-GR24 or (±)-contalactone, respectively. Protein + ligand in PBS buffer (pH 6.8) for 150 min at 22 °C. (**B**) Chemical hydrolysis of (±)-contalactone and (±)-GR24 in ethanol/water at pH 6.8. Data are means ± SE (n = 3).

Figure 3. Length of the axillary buds of *rms1-10* and *rms3-5* pea plants, 8 d after direct application of (±)-GR24 or (±)-contalactone (= (±)-contalac.) ; CTL0 = DMSO treatment ; WT Térèse plants were used as controls without treatment. Data are means ± SE (≥20 plants). *$P < 0.05$; ***$P < 0.001$, Kruskal-Wallis rank sum test, compared to CTL0 value.

Figure 4. Biochemical analysis of the interaction between the RMS3 protein and (±)-contalactone. (**A**) Melting temperature curves for RMS3 at indicated concentrations of (±)-GR24, P270 and (±)-contalactone, as assessed by DSF. Each line represents the average protein melting curve for three technical replicates and the experiment was carried out three times. (**B**) Changes in intrinsic fluorescence emission spectra of RMS3 in the presence of various concentrations of (±)-GR24, P270 or (±)-contalactone. (**C**) Intrinsic tryptophan fluorescence of RMS3 protein in the presence of SL analogs. Plots of fluorescence intensity *versus* (±)-GR24 or (±)-contalactone concentrations were used to determine the apparent K_D values. The plots represent the mean of two replicates and the experiments were repeated at least three times.

Figure 5. Effect of (±)-GR24, (±)-270 and (±)-contalactone on hypocotyl elongation in *Col-0, max3-11, Atd14-1, htl3* and *max2-1 Arabidopsis* plants. Data are means ± SE (n = 14 plants). ***$P < 0.001$, Kruskal-Wallis rank sum test, compared to control values (CTL0).

Figure 6. Germination Stimulation (GS) activity on seeds of *P. ramosa, O. cumana* and *S. hermonthica* by (±)-contalactone. Comparison with GR24 isomers, dehydrocostus lactone (DCL) and 2-phenethyl isothiocyanate (2-PEITC). (**A**) Maximum of Germination Stimulant activity relative to (±)-GR24 (1 µM). Data are presented ± SE. (**B**) EC_{50} (half maximal effective concentration) ($mol.L^{-1}$) of (±)-contalactone, GR24 isomers, DCL and 2-PEITC

toward *Phelipanche ramosa* (1 and 2a), *Orobanche cumana*, *Striga hermonthica* root parasitic plant seed germination. EC_{50} are presented ± SE.

Figure 7. Effect of (±)-contalactone on symbiotic ability of the AM fungus *Rhizophagus irregularis*. This fungus was inoculated on *Medicago truncatula* SL-deficient mutants, in the absence (CTL0) or presence of SL analogs at 10^{-7} M. The number of infection points was recorded three weeks post-inoculation. Bars represent the mean ± SE of 9-12 replicates per condition. ***$P < 0.001$, ** $P < 0.01$, Mann-Whitney test, compared to control values (CTL0).

References

Akiyama, K., Matsuzaki, K., Hayashi, H., 2005. Plant sesquiterpenes induce hyphal branching in arbuscular mycorrhizal fungi. Nature 435, 824-827.

Akiyama, K., Ogasawara, S., Ito, S., Hayashi, H., 2010. Structural Requirements of Strigolactones for Hyphal Branching in AM Fungi. Plant Cell Physiol. 51, 1104-1117.

Auger, B., Pouvreau, J.-B., Pouponneau, K., Yoneyama, K., Montiel, G., Le Bizec, B., Yoneyama, K., Delavault, P., Delourme, R., Simier, P., 2012. Germination Stimulants of Phelipanche ramosa in the Rhizosphere of Brassica napus Are Derived from the Glucosinolate Pathway. Mol. Plant-Microbe Interact. 25, 993-1004.

Besserer, A., Puech-Pages, V., Kiefer, P., Gomez-Roldan, V., Jauneau, A., Roy, S., Portais, J. C., Roux, C., Bécard, G., Sejalon-Delmas, N., 2006. Strigolactones stimulate arbuscular mycorrhizal fungi by activating mitochondria. PLoS. Biol. 4, 1239-1247.

Boyer, F.-D., de Saint Germain, A., Pillot, J.-P., Pouvreau, J.-B., Chen, V. X., Ramos, S., Stévenin, A., Simier, P., Delavault, P., Beau, J.-M., Rameau, C., 2012. Structure-Activity Relationship Studies of Strigolactone-Related Molecules for Branching Inhibition in Garden Pea: Molecule Design for Shoot Branching. Plant Physiol. 159, 1524-1544.

Braun, N., de Saint Germain, A., Pillot, J. P., Boutet-Mercey, S., Dalmais, M., Antoniadi, I., Li, X., Maia-Grondard, A., Le Signor, C., Bouteiller, N., Luo, D., Bendahmane, A., Turnbull, C., Rameau, C., 2012. The pea TCP transcription factor PsBRC1 acts downstream of Strigolactones to control shoot branching. Plant Physiol. 158, 225-238.

Bromhead, L. J., McErlean, C. S. P., 2017. Accessing Single Enantiomer Strigolactones: Progress and Opportunities. Eur. J. Org. Chem. 2017, 5712-5723.

Cook, C. E., Whichard, L. P., Turner, B., Wall, M. E., 1966. Germination of Witchweed (Striga Lutea Lour) - Isolation and Properties of a Potent Stimulant. Science 154, 1189-1190.

de Saint Germain, A., Clavé, G., Badet-Denisot, M.-A., Pillot, J.-P., Cornu, D., Le Caer, J.-P., Burger, M., Pelissier, F., Retailleau, P., Turnbull, C., Bonhomme, S., Chory, J., Rameau, C.,

Boyer, F.-D., 2016. An histidine covalent receptor and butenolide complex mediates strigolactone perception. Nat. Chem. Biol. 12, 787-794.

Fox, J., 2005. The R commander: A basic-statistics graphical user interface to R. Journal of Statistical Software 14, 1-42.

Gomez-Roldan, V., Fermas, S., Brewer, P. B., Puech-Pages, V., Dun, E. A., Pillot, J.-P., Letisse, F., Matusova, R., Danoun, S., Portais, J.-C., Bouwmeester, H., Bécard, G., Beveridge, C. A., Rameau, C., Rochange, S. F., 2008. Strigolactone inhibition of shoot branching. Nature 455, 189-194.

Hamiaux, C., Drummond, R. S. M., Janssen, B. J., Ledger, S. E., Cooney, J. M., Newcomb, R. D., Snowden, K. C., 2012. DAD2 Is an alpha/beta Hydrolase Likely to Be Involved in the Perception of the Plant Branching Hormone, Strigolactone. Curr. Biol. 22, 2032-2036.

Joel, D. M., Chaudhuri, S. K., Plakhine, D., Ziadna, H., Steffens, J. C., 2011. Dehydrocostus lactone is exuded from sunflower roots and stimulates germination of the root parasite Orobanche cumana. Phytochemistry 72, 624-634.

Johnson, A. W., Gowda, G., Hassanali, A., Knox, J., Monaco, S., Razavi, Z., Rosebery, G., 1981. The Preparation of Synthetic Analogs of Strigol. J. Chem. Soc., Perkin Trans. 1, 1734-1743.

Lauressergues, D., André, O., Peng, J., Wen, J., Chen, R., Ratet, P., Tadege, M., Mysore, K. S., Rochange, S. F., 2015. Strigolactones contribute to shoot elongation and to the formation of leaf margin serrations in Medicago truncatula R108. J. Exp. Bot. 66, 1237-1244.

Lopez-Obando, M., Ligerot, Y., Bonhomme, S., Boyer, F. D., Rameau, C., 2015. Strigolactone biosynthesis and signaling in plant development. Development 142, 3615-3619.

Mangnus, E. M., Dommerholt, F. J., Dejong, R. L. P., Zwanenburg, B., 1992. Improved Synthesis of Strigol Analog GR24 and Evaluation of the Biological-Activity of Its Diastereomers. J. Agric. Food. Chem. 40, 1230-1235.

Mori, N., Nishiuma, K., Sugiyama, T., Hayashi, H., Akiyama, K., 2016. Carlactone-type strigolactones and their synthetic analogues as inducers of hyphal branching in arbuscular mycorrhizal fungi. Phytochemistry 130, 90-98.

Nelson, D. C., Scaffidi, A., Dun, E. A., Waters, M. T., Flematti, G. R., Dixon, K. W., Beveridge, C. A., Ghisalberti, E. L., Smith, S. M., 2011. F-box protein MAX2 has dual roles in karrikin and strigolactone signaling in *Arabidopsis thaliana*. Proc. Natl. Acad. Sci. U.S.A. 108, 8897-8902.

Pouvreau, J.-B., Gaudin, Z., Auger, B., Lechat, M. M., Gauthier, M., Delavault, P., Simier, P., 2013. A high-throughput seed germination assay for root parasitic plants. Plant Methods 9, 32.

Rameau, C., Bodelin C, Cadier D, Grandjean O, Miard F, Murfet IC, 1997. New *ramosus* mutants at loci *Rms1*, *Rms3* and *Rms4* resulting from the mutation breeding program at Versailles. Pisum Genetics 29, 7-12.

Rigaku, O. D., 2015. CrysAlis PRO. Rigaku Oxford Diffraction Ltd, Yarnton, England.

Seto, Y., Yasui, R., Kameoka, H., Tamiru, M., Cao, M., Terauchi, R., Sakurada, A., Hirano, R., Kisugi, T., Hanada, A., Umehara, M., Seo, E., Akiyama, K., Burke, J., Takeda-Kamiya, N., Li, W., Hirano, Y., Hakoshima, T., Mashiguchi, K., Noel, J. P., Kyozuka, J., Yamaguchi, S., 2019. Strigolactone perception and deactivation by a hydrolase receptor DWARF14. Nat Commun 10, 191.

Shabek, N., Ticchiarelli, F., Mao, H., Hinds, T. R., Leyser, O., Zheng, N., 2018. Structural plasticity of D3–D14 ubiquitin ligase in strigolactone signalling. Nature 563, 652-656.

Sheldrick, G. M., 2015a. Crystal structure refinement with SHELXL. Acta Crystallogr., Sect. C: Cryst. Struct. Commun. 71, 3-8.

Sheldrick, G. M., 2015b. SHELXT - Integrated space-group and crystal-structure determination. Acta Crystallogr., Sect. A: Found. Crystallogr. 71, 3-8.

Stirnberg, P., van de Sande, K., Leyser, H. M. O., 2002. MAX1 and MAX2 control shoot lateral branching in Arabidopsis. Development 129, 1131-1141.

Stojanova, B., Delourme, R., Duffé, P., Delavault, P., Simier, P., 2019. Genetic differentiation and host preference reveal non-exclusive host races in the generalist parasitic weed Phelipanche ramosa. Weed Res. 59, 107-118.

Takahashi, I., Asami, T., 2018. Target-based selectivity of strigolactone agonists and antagonists in plants and their potential use in agriculture. J. Exp. Bot. 69, 2241-2254.

Thuring, J., vanGaal, A., Hornes, S. J., deKok, M. M., Nefkens, G. H. L., Zwanenburg, B., 1997. Synthesis and biological evaluation of strigol analogues modified in the enol ether part. J. Chem. Soc., Perkin Trans. 1, 767-774.

Toh, S., Holbrook-Smith, D., Stokes, M. E., Tsuchiya, Y., McCourt, P., 2014. Detection of Parasitic Plant Suicide Germination Compounds Using a High-Throughput Arabidopsis HTL/KAI2 Strigolactone Perception System. Chem Biol 21, 988-998.

Umehara, M., Hanada, A., Yoshida, S., Akiyama, K., Arite, T., Takeda-Kamiya, N., Magome, H., Kamiya, Y., Shirasu, K., Yoneyama, K., Kyozuka, J., Yamaguchi, S., 2008. Inhibition of shoot branching by new terpenoid plant hormones. Nature 455, 195-200.

Waters, M. T., Gutjahr, C., Bennett, T., Nelson, D. C., 2017. Strigolactone Signaling and Evolution. Annu. Rev. Plant Biol. 68, 291-322.

Waters, M. T., Nelson, D. C., Scaffidi, A., Flematti, G. R., Sun, Y. K., Dixon, K. W., Smith, S. M., 2012. Specialisation within the DWARF14 protein family confers distinct responses to karrikins and strigolactones in *Arabidopsis*. Development 139, 1285-1295.

Xie, X., Yoneyama, K., Yoneyama, K., 2010. The Strigolactone Story. Annu. Rev. Phytopathol. 48, 93-117.

Yao, R., Ming, Z., Yan, L., Li, S., Wang, F., Ma, S., Yu, C., Yang, M., Chen, L., Li, Y., Yan, C., Miao, D., Sun, Z., Yan, J., Sun, Y., Wang, L., Chu, J., Fan, S., He, W., Deng, H., Nan, F., Li, J., Rao, Z., Lou, Z., Xie, D., 2016. DWARF14 is a non-canonical hormone receptor for strigolactone. Nature 536, 469-473.

Yasui, M., Ota, R., Tsukano, C., Takemoto, Y., 2017. Total synthesis of avenaol. Nat. Commun. 8, 674.

Yoneyama, K., Xie, X., Yoneyama, K., Kisugi, T., Nomura, T., Nakatani, Y., Akiyama, K., McErlean, C. S. P., 2018. Which are the major players, canonical or non-canonical strigolactones? J. Exp. Bot. 69, 2231-2239.

Zhao, L.-H., Zhou, X. E., Yi, W., Wu, Z., Liu, Y., Kang, Y., Hou, L., de Waal, P. W., Li, S., Jiang, Y., Scaffidi, A., Flematti, G. R., Smith, S. M., Lam, V. Q., Griffin, P. R., Wang, Y., Li, J., Melcher, K., Xu, H. E., 2015. Destabilization of strigolactone receptor DWARF14 by binding of ligand and E3-ligase signaling effector DWARF3. Cell Res. 25, 1219-1236.

Zwanenburg, B., Cavar Zeljkovic, S., Pospisil, T., 2016a. Synthesis of strigolactones, a strategic account. Pest Manage. Sci. 72, 15-29.

Zwanenburg, B., Mwakaboko, A. S., 2011. Strigolactone analogues and mimics derived from phthalimide, saccharine, p-tolylmalondialdehyde, benzoic and salicylic acid as scaffolds. Bioorg. Med. Chem. 19, 7394-7400.

Zwanenburg, B., Nayak, S. K., Charnikhova, T. V., Bouwmeester, H. J., 2013. New strigolactone mimics: structure-activity relationship and mode of action as germinating stimulants for parasitic weeds. Bioorg. Med. Chem. Lett. 23, 5182-5186.

Zwanenburg, B., Pospisil, T., Zeljkovic, S. C., 2016b. Strigolactones: new plant hormones in action. Planta 243, 1311-1326.

Figure 1

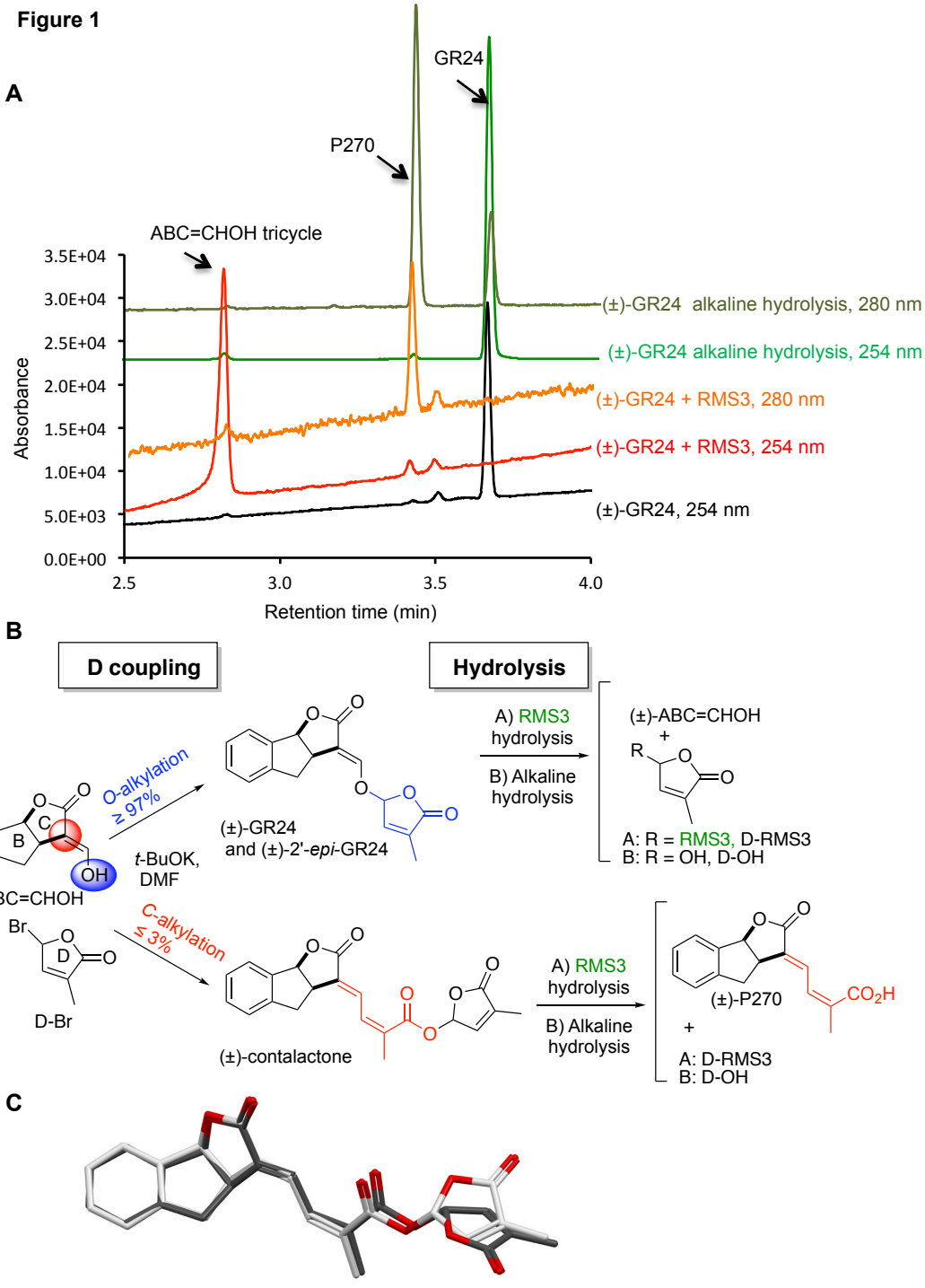
A
GR24
P270
ABC=CHOH tricycle
3.5E+04
3.0E+04
2.5E+04
2.0E+04
1.5E+04
1.0E+04
5.0E+03
0.0E+00
Absorbance
2.5
3.0
3.5
4.0
Retention time (min)
(±)-GR24 alkaline hydrolysis, 280 nm
(±)-GR24 alkaline hydrolysis, 254 nm
(±)-GR24 + RMS3, 280 nm
(±)-GR24 + RMS3, 254 nm
(±)-GR24, 254 nm
B
D coupling
Hydrolysis
O-alkylation
≥ 97%
t-BuOK,
DMF
(±)-ABC=CHOH
(±)-GR24
and (±)-2'-epi-GR24
A) RMS3
hydrolysis
B) Alkaline
hydrolysis
(±)-ABC=CHOH
A: R = RMS3, D-RMS3
B: R = OH, D-OH
C-alkylation
≤ 3%
D-Br
(±)-contalactone
(±)-P270
A: D-RMS3
B: D-OH
C

Figure 2

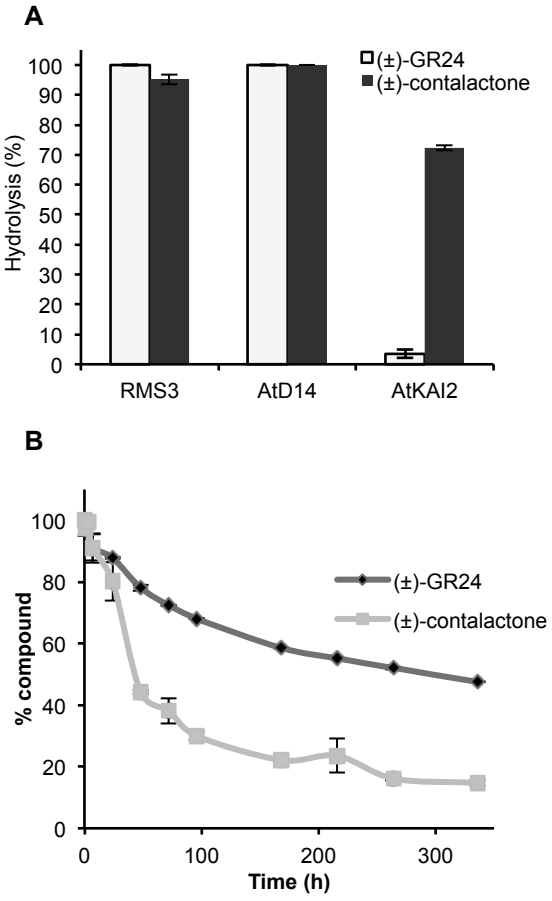
A
(±)-GR24
(±)-contalactone
Hydrolysis (%)
100
90
80
70
60
50
40
30
20
10
0
RMS3
AtD14
AtKAI2
B
(±)-GR24
(±)-contalactone
% compound
100
80
60
40
20
0
0
100
200
300
Time (h)

Figure 3

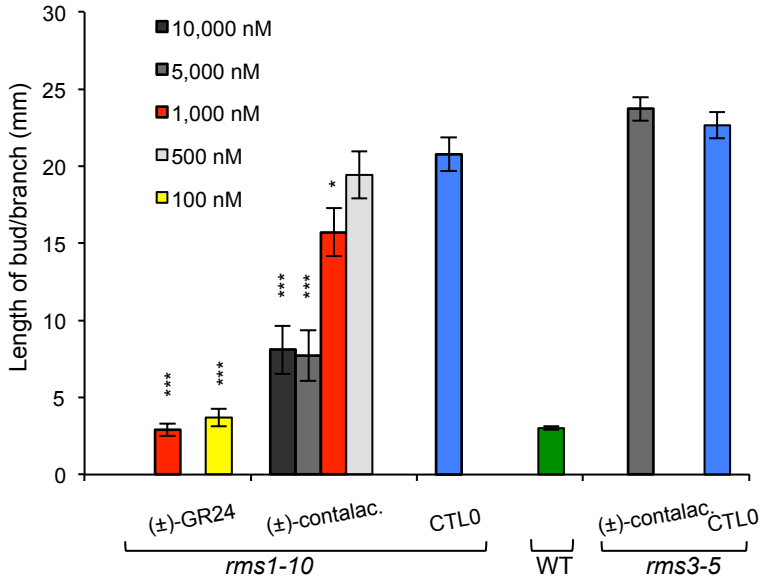
Length of bud/branch (mm)
30
25
20
15
10
5
0
10,000 nM
5,000 nM
1,000 nM
500 nM
100 nM
***
***
***
***
*
(±)-GR24
(±)-contalac.
CTL0
(±)-contalac.
CTL0
rms1-10
WT
rms3-5

Figure 4

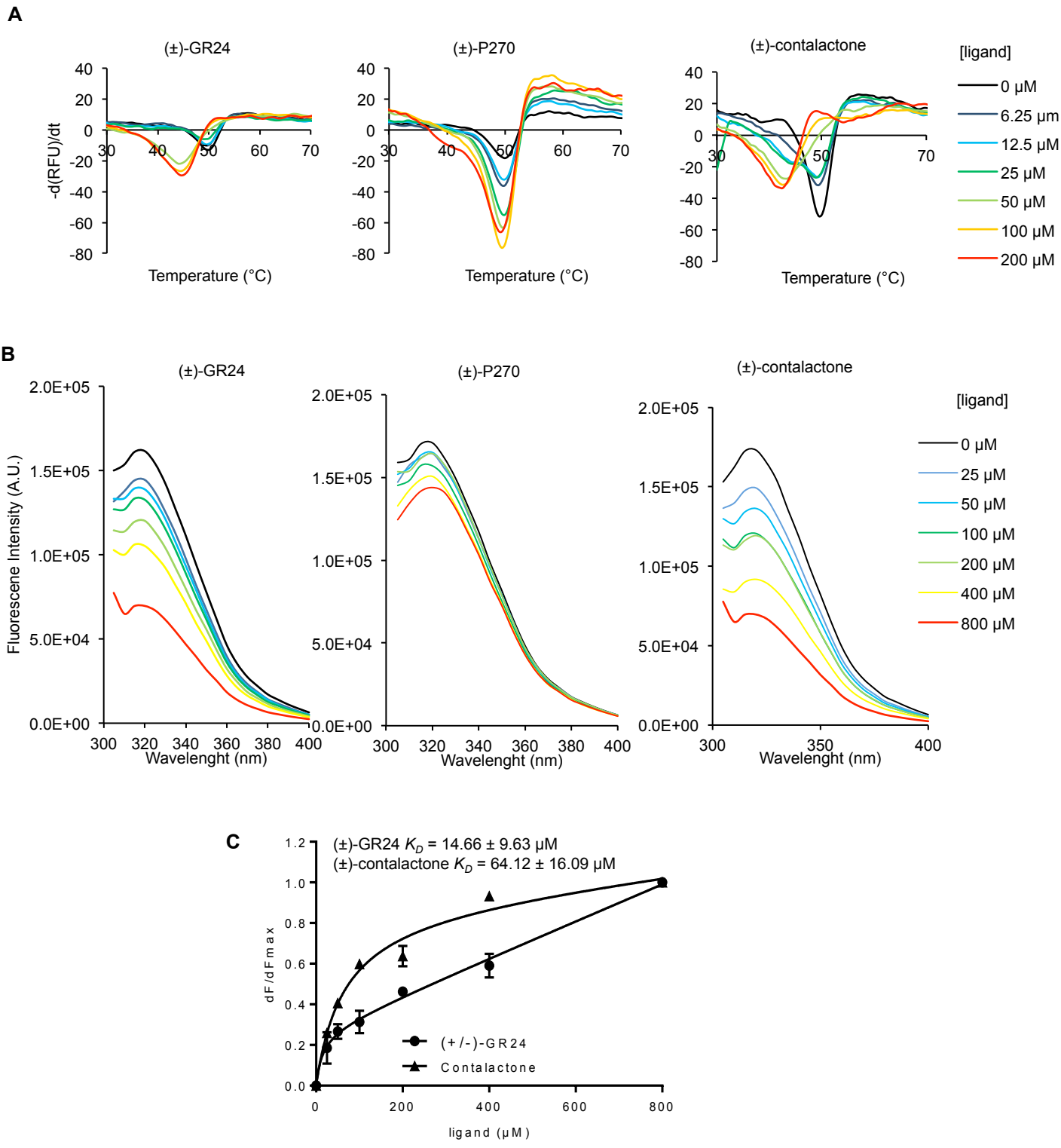
A
(±)-GR24
(±)-P270
(±)-contalactone
-d(RFU)/dt
Temperature (°C)
[ligand]
0 µM
6.25 µm
12.5 µM
25 µM
50 µM
100 µM
200 µM
B
(±)-GR24
(±)-P270
(±)-contalactone
Fluorescene Intensity (A.U.)
Wavelenght (nm)
[ligand]
0 µM
25 µM
50 µM
100 µM
200 µM
400 µM
800 µM
C
(±)-GR24 K_D = 14.66 ± 9.63 µM
(±)-contalactone K_D = 64.12 ± 16.09 µM
dF/dFmax
ligand (µM)
(+/-)-GR24
Contalactone

Figure 5

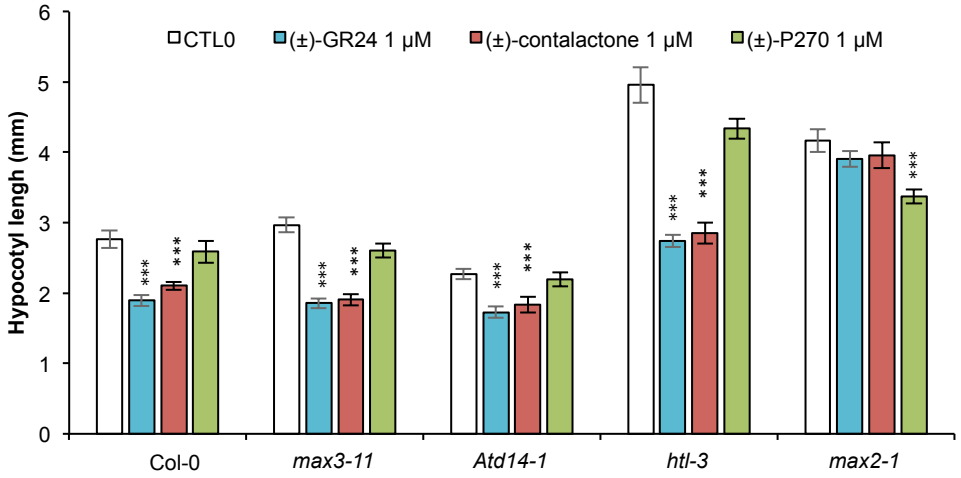
CTL0
(±)-GR24 1 µM
(±)-contalactone 1 µM
(±)-P270 1 µM
Hypocotyl lengh (mm)
0
1
2
3
4
5
6
Col-0
max3-11
Atd14-1
htl-3
max2-1

Figure 6

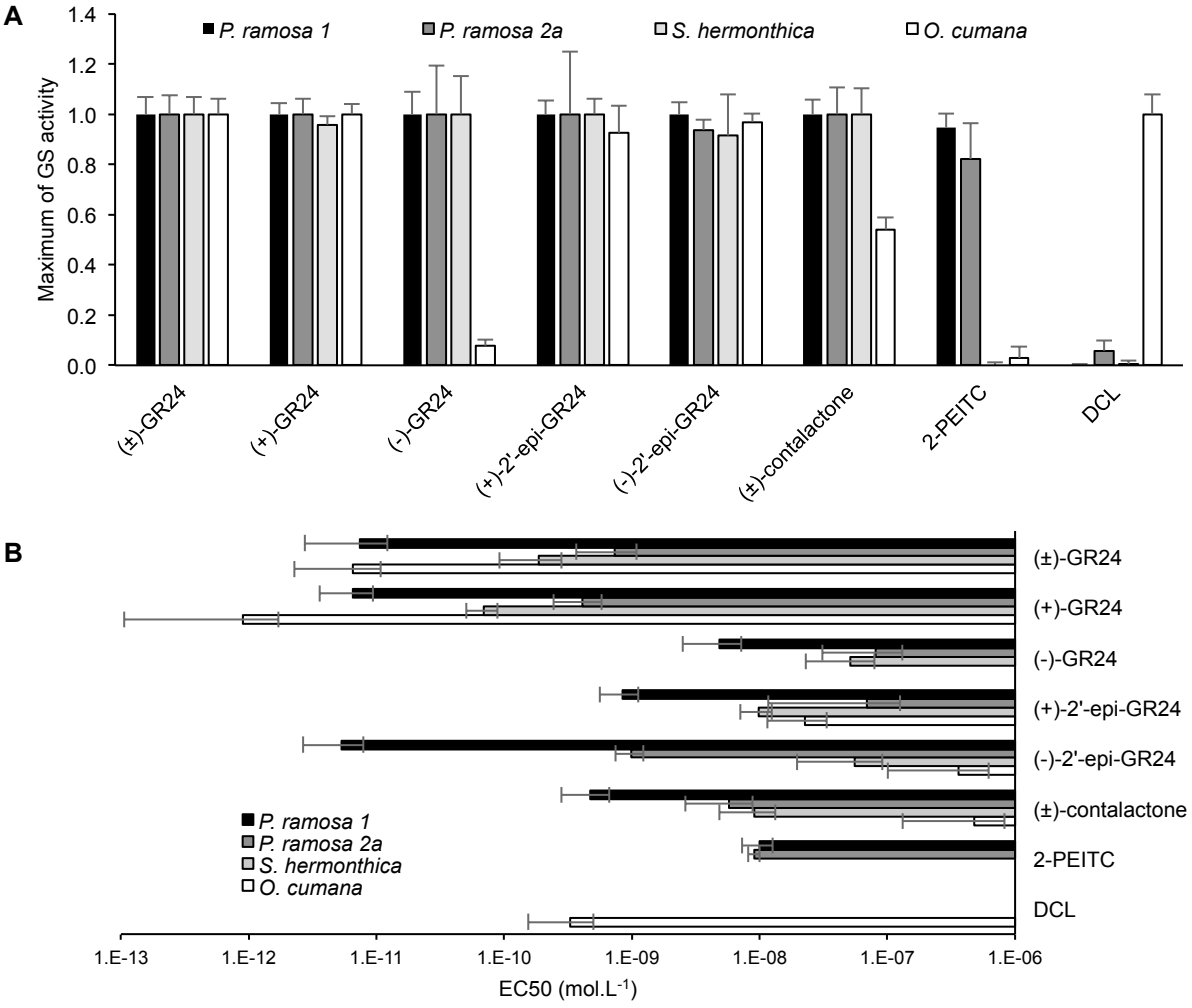
A
P. ramosa 1
P. ramosa 2a
S. hermonthica
O. cumana
Maximum of GS activity
1.4
1.2
1.0
0.8
0.6
0.4
0.2
0.0
(±)-GR24
(+)-GR24
(-)-GR24
(+)-2'-epi-GR24
(-)-2'-epi-GR24
(±)-contalactone
2-PEITC
DCL
B
(±)-GR24
(+)-GR24
(-)-GR24
(+)-2'-epi-GR24
(-)-2'-epi-GR24
(±)-contalactone
2-PEITC
DCL
P. ramosa 1
P. ramosa 2a
S. hermonthica
O. cumana
1.E-13
1.E-12
1.E-11
1.E-10
1.E-09
1.E-08
1.E-07
1.E-06
EC50 (mol.L-1)

Figure 7

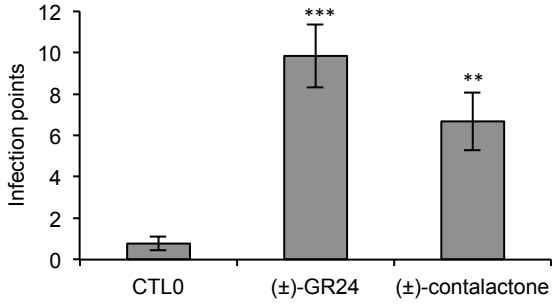

Supplementary Tables

Supplementary Table 1. Conditions for the preparation of (±)-GR24 isomers and (±)-contalactone. [a] Measured by ^{1}H NMR and UPLC-DAD analysis of the crude reaction mixture.

Entry	Conditions	Ratio (GR24/2'-*epi*-GR24 : contalactone)[a]
1	1) *t*BuOK, THF, 0 °C, 1 h 2) D-Br, DMF −70 °C to rt, 17 h	>97: 3
2	1) K_2CO_3, acetone, 0 °C, 40 min 2) D-Br, acetone, −70 °C to rt, 17 h	94: 6
3	1) K_2CO_3, acetone, 0 °C, 10 min 2) 2) D-Br, acetone, rt, 4 h	93: 7
4	1) K_2CO_3, acetone, rt, 15 min 2) D-Br, acetone, reflux, 12 h	91: 9
5	1) D-Br, K_2CO_3, toluene, 55 °C, 2 h 30	92: 8

Supplementary Table 2. Experimental details for X-ray analysis of contalactone (FDB2980F1).

Identification code		FDB2980F1 – diastereomer 1	FDB2980F1 – diastereomer 2
Empirical formula		$C_{21}H_{18}O_6$	$C_{21}H_{18}O_6$
Formula weight		366.35	366.35
Temperature (K)		173(2)	173(2)
Wavelength (Å)		0.71073	0.71073
Crystal system, Space group		Monoclinic, $P\ 2_1/c$	Triclinic, P -1
Unit cell dimensions	a (Å)	18.1868(12)	7.811(2)
	b	14.0611(13)	10.187(3)
	c	6.8870(4)	12.717(10)
	α (°)	90	112.22(5)
	β	94.276(6)	104.93(5)
	γ	90	93.47(2)
Volume ($Å^3$)		1756.3(2)	890.9(8)
Z, Calculated density (Mg/m^3)		4, 1.386	2, 1.366
Absorption coefficient (mm^{-1})		0.102	0.101
F(000)		768	384
Crystal habit		Elongated platelet	Squared tab
Crystal size (mm)		0.26 x 0.09 x 0.03	0.12 x 0.10 x 0.05
θ range for data collection (°)		3.558 to 26.732	2.742 to 25.350
Limiting indices		$-23 \le h \le 23$, $-17 \le k \le 17$, $-8 \le l \le 8$	$-9 \le h \le 9$, $-12 \le k \le 11$, $-15 \le l \le 15$
Reflections collected / unique R(int)		20087 / 3717 0.0854	11480 / 3240 0.060
Completeness to θ_{full} (%)		99.7	99.0
Absorption correction		Semi-empirical from equivalents	Semi-empirical from equivalents
Max. and min. transmission		1.000 and 0.537	1.000 and 0.434
Refinement method		Full-matrix least-squares on F^2	Full-matrix least-squares on F^2
Data / restraints / parameters		3714 / 0 / 246	3233 / 0 / 246
Goodness-of-fit on F^2		1.098	1.083
Final R indices [I>2σ(I)]	R1	0.0623,	0.0797,
	wR2	0.1210	0.2285
R indices (all data)	R1	0.0834,	0.0981,
	wR2	0.1293	0.2459
Largest Δ peak and hole ($e.Å^{-3}$)		0.255 and -0.197	0.646 and -0.487
CCDC deposit number		1870390	1870391

Supplementary Table 3. Bud outgrowth inhibition activity assay results for SL derivatives. [a] Data are means ± SE ($n \geq 20$), 8 days after treatment of *rms1-10* pea plants. [b] Comparison of the treatment to the control treatment (0 nM) using the Kruskal-Wallis rank sum test.

Compound (no. of replicates)	Concentration	Length of bud at node 3 /branch (mm)[a]	p-value
(±)-GR24	1,000 nM	1.90 ± 0.08	0.00e-00 [b]
	1,000 nM	1.80 ± 0.11	0.00e-00 [b]
	1,000 nM	3.18 ± 0.50	0.00e-00 [b]
	1,000 nM	2.82 ± 0.22	0.00e-00 [b]
	1,000 nM	3.65 ± 0.69	0.00e-00 [b]
	1,000 nM	2.89 ± 0.39	0.00e-00 [b]
	100 nM	3.03 ± 0.83	1.09e-03 [b]
	100 nM	1.97 ± 0.10	0.00e-00 [b]
	100 nM	7.60 ± 2.53	2.40e-07 [b]
	100 nM	4.58 ± 1.11	0.00e-00 [b]
	100 nM	3.69 ± 0.56	0.00e-00 [b]
	10 nM	6.37 ± 1.01	2.99e-03 [b]
(±)-Contalactone	10,000 nM	3.31 ± 1.57	0.00e-00 [b]
	10,000 nM	8.09 ± 1.57	1.09e-11 [b]
	5,000 nM	8.20 ± 1.43	4.12e-11 [b]
	5,000 nM	7.72 ± 1.65	5.55e-15 [b]
	1,000 nM	13.35 ± 1.82	0.00e-00 [b]
	1,000 nM	14.73 ± 1.62	6.91e-01 [b]
	1,000 nM	15.73 ± 1.58	3.35e-02 [b]
	500 nM	19.34 ± 0.78	9.97e-01 [b]
	500 nM	19.45 ± 1.54	9.9989e-01 [b]
	100 nM	26.63 ± 1.15	0.46e+00 [b]
	100 nM	18.41 ± 0.87	9.9989e-01 [b]
(±)-P270	10,000 nM	8.80 ± 1.17	8.31e-01 [b]
	1,000 nM	10.66 ± 1.06	1.00e+00 [b]
	1,000 nM	12.44 ± 2.29	3.44e-01 [b]
	1,000 nM	8.77 ± 2.03	9.94e-01 [b]
	100 nM	11.23 ± 2.65	9.49e-01 [b]
	100 nM	5.80 ± 1.31	5.22e-01 [b]
ABC=CHOH	10,000 nM	13.00 ± 1.78	1.00e+00 [b]
	1,000 nM	10.39 ± 1.09	9.63e-01 [b]

Supplementary Table 4. Bud outgrowth inhibition activity assay for (±)-contalactone and (±)-GR24. [a] Data are means ± SE ($n \geq 20$), 8 days after treatment of *rms3-5* pea plants. [b] Comparison of the treatment to the control treatment (0 nM) using the Kruskal-Wallis rank sum test.

Compound (no. of replicates)	Concentration	Length of bud at node 3 /branch (mm)[a]	p-value
(±)-GR24	5,000 nM	21.44 ± 1.21	0.9999897 [b]
	5,000 nM	18.78 ± 1.30	0.9972101 [b]
(±)-Contalactone	10,000 nM	20.98 ± 2.27	5.862260e-02 [b]
	5,000 nM	19.44 ± 1.30	0.8567548 [b]
	5,000 nM	23.73 ± 0.77	0.6399994 [b]

Supplementary Figures

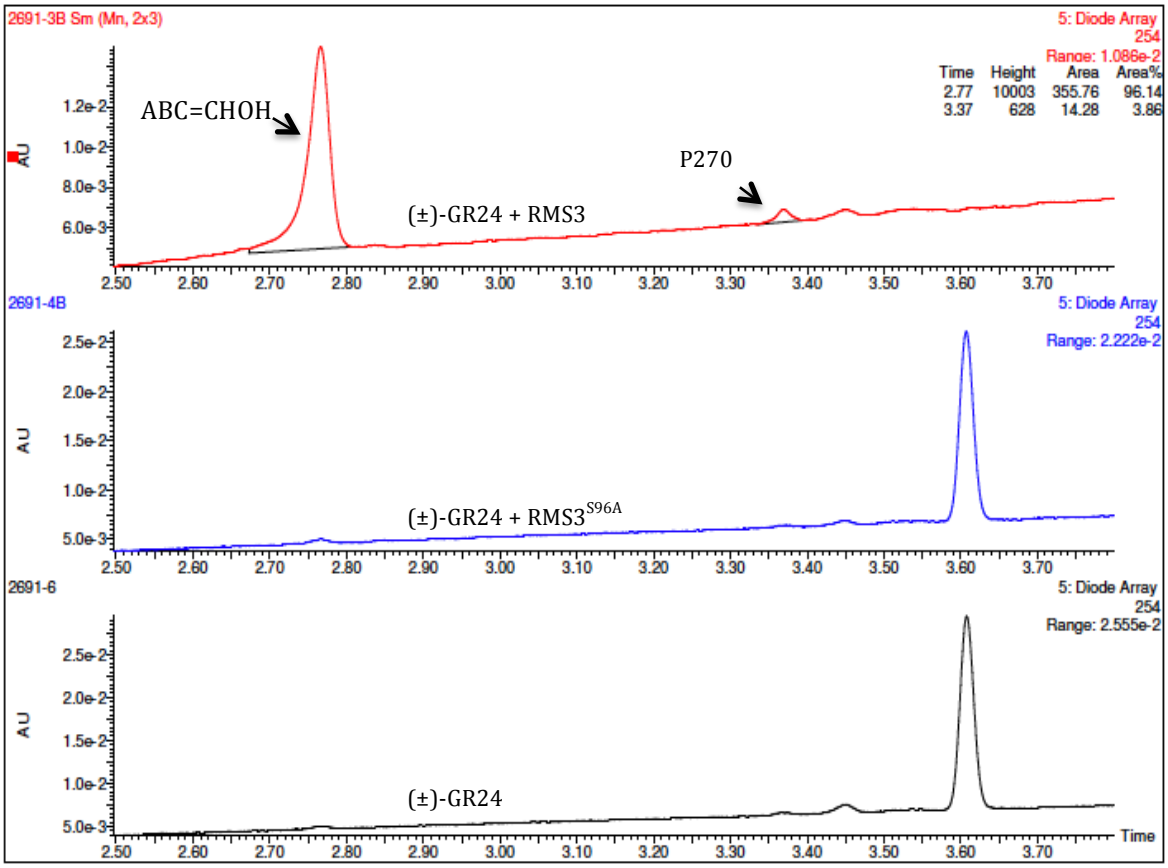

Supplementary Figure 1. Detection of the novel compound (P270) following enzymatic activity of the SL receptor from (±)-GR24 prepared according to (Mangnus *et al.*, 1992). Elution profile of the enzymatic assay with buffer (pH 6.8), RMS3, RMS3^{S96A} and (±)-GR24 purified by flash chromatography on silica gel. UPLC with diode array detection (200-400 nm) shows the formation of ABC=CHOH and compound P270. (±)-Contalactone is not detected.

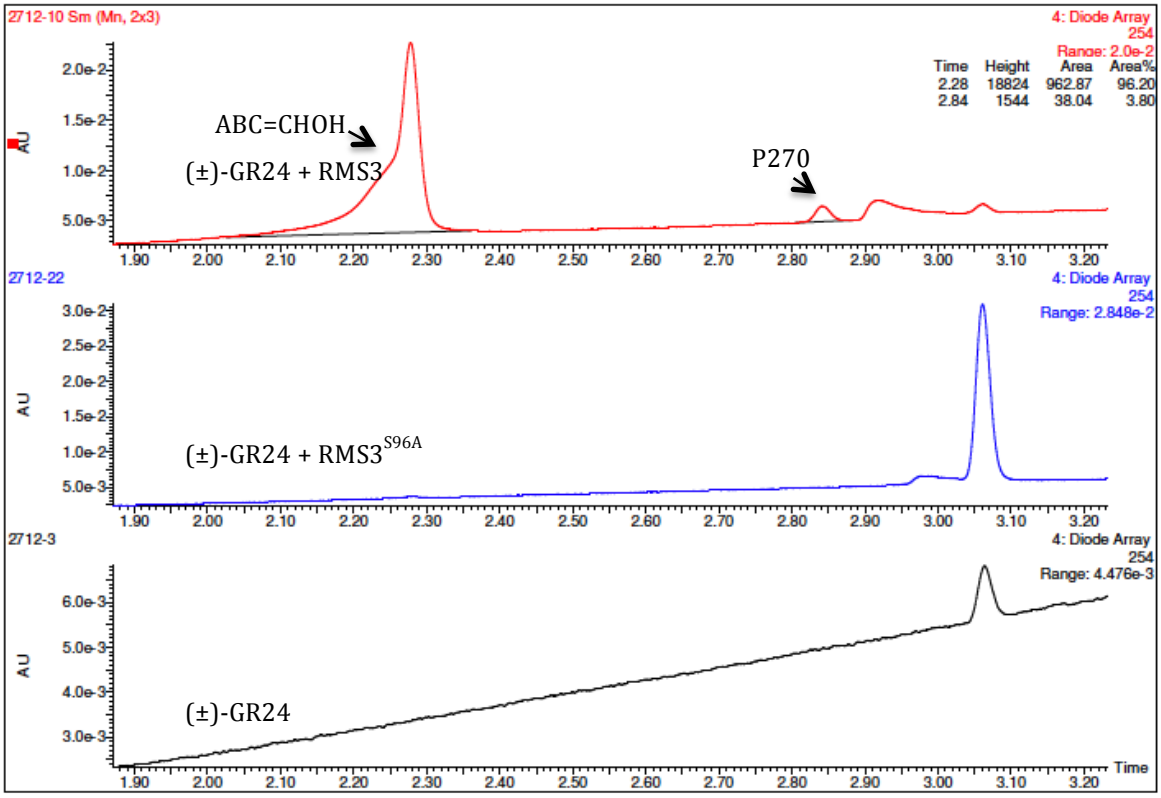

Supplementary Figure 2. Detection of the novel compound (P270) following enzymatic activity of the SL receptor from (±)-GR24 purchased from supplier #1. Elution profile of the enzymatic assay with buffer (pH 6.8), RMS3, RMS3^{S96A} and (±)-GR24 purchased from supplier #1. UPLC with diode array detection (200-400 nm) shows the formation of ABC=CHOH and compound P270. (±)-Contalactone is not detected.

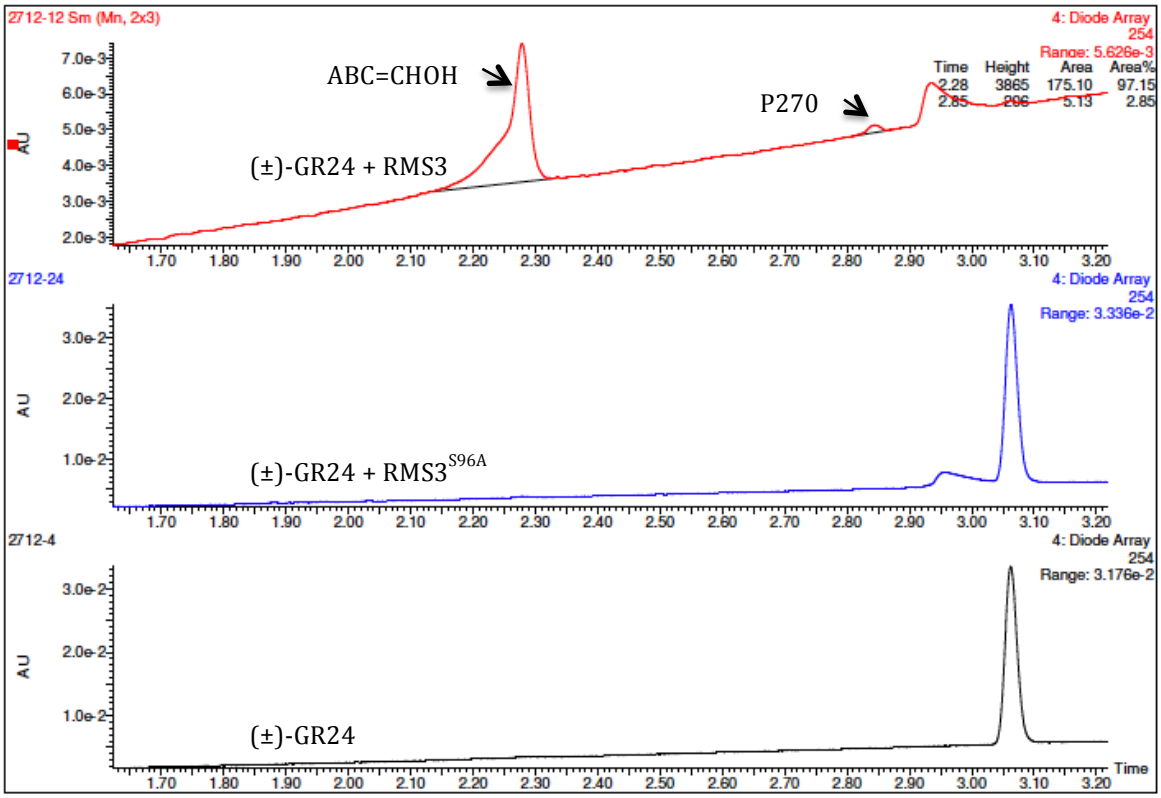

Supplementary Figure 3. Detection of the novel compound (P270) following enzymatic activity of the SL receptor from (±)-GR24 purchased from supplier #2. Elution profile of the enzymatic assay with buffer (pH 6.8), RMS3, RMS3^{S96A} and (±)-GR24 purchased from supplier #2. UPLC with diode array detection (200-400 nm) shows the formation of ABC=CHOH and compound P270. (±)-Contalactone is not detected.

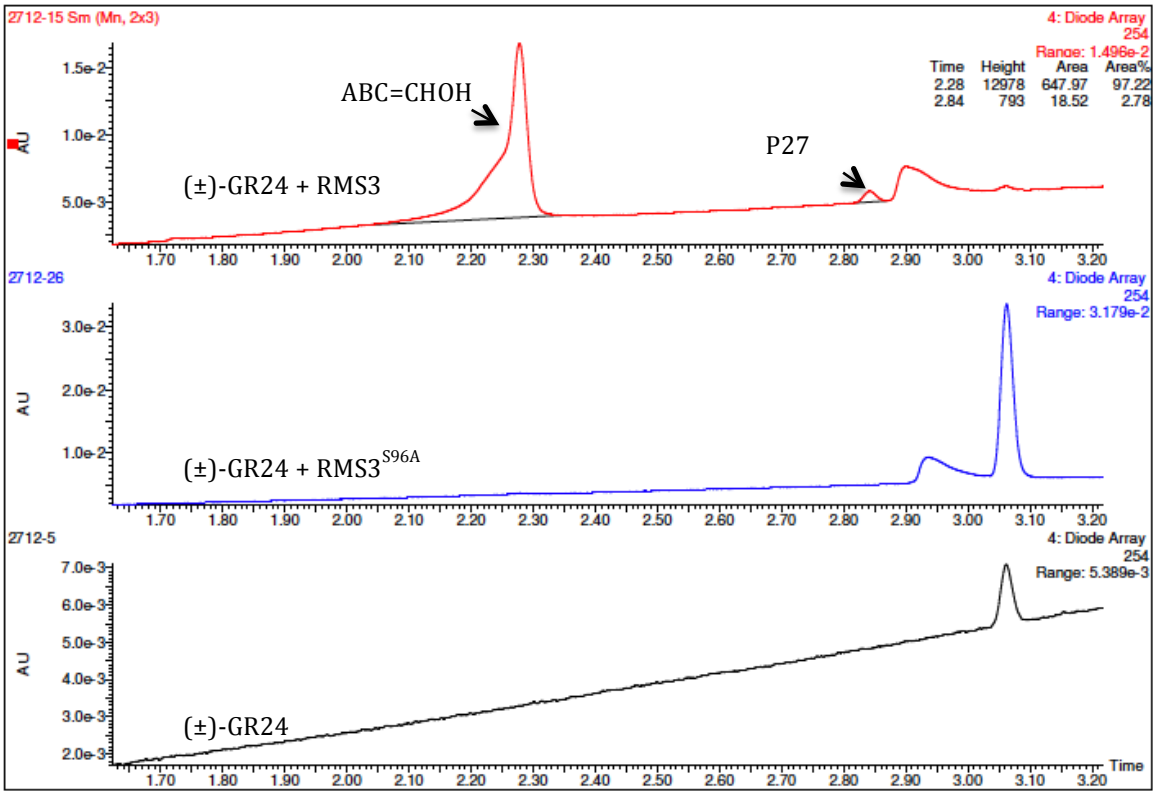

Supplementary Figure 4. Detection of the novel compound (P270) following enzymatic activity of the SL receptor from (±)-GR24 purchased from supplier #3. Elution profile of the enzymatic assay with buffer (pH 6.8), RMS3, RMS3^{S96A} and (±)-GR24 purchased from supplier #3. UPLC with diode array detection (200-400 nm) shows the formation of ABC=CHOH and compound P270. (±)-Contalactone is not detected.

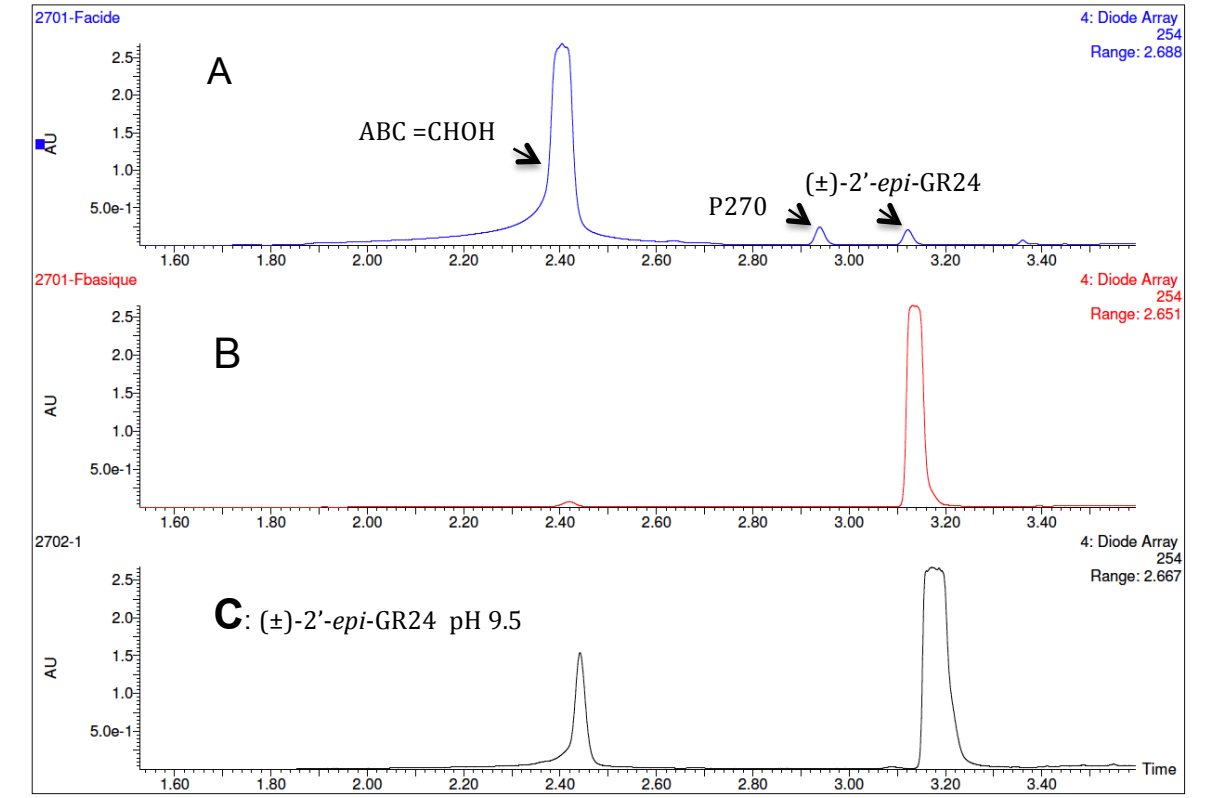

Supplementary Figure 5. Characterization of P270 by HPLC analysis. (**A**) Elution profile of the aqueous phase obtained after the chemical hydrolysis with buffer (pH 9.5) of (±)-2'-*epi*-GR24 prepared according to (Mangnus *et al.*, 1992) and washed with CH_2Cl_2. UPLC with diode array detection (200-400 nm) shows ABC=CHOH and P270 and traces of (±)-2'-*epi*-GR24. (**B**) Elution profile of CH_2Cl_2 phase obtained after the chemical hydrolysis with buffer (pH 9.5) of (±)-2'-*epi*-GR24 prepared according to (Mangnus *et al.*, 1992). UPLC with diode array detection (200-400 nm) shows (±)-2'-*epi*-GR24 as major compound, the presence of traces of ABC=CHOH and no compound P270. (**C**) Elution profile of the chemical hydrolysis with buffer (pH 9.5) of (±)-2'-*epi*-GR24 obtained by a first chemical hydrolysis at pH 9.5 and extraction with CH_2Cl_2. UPLC with diode array detection (200-400 nm) shows the formation of ABC=CHOH and no compound P270. (±)-Contalactone is not detected.

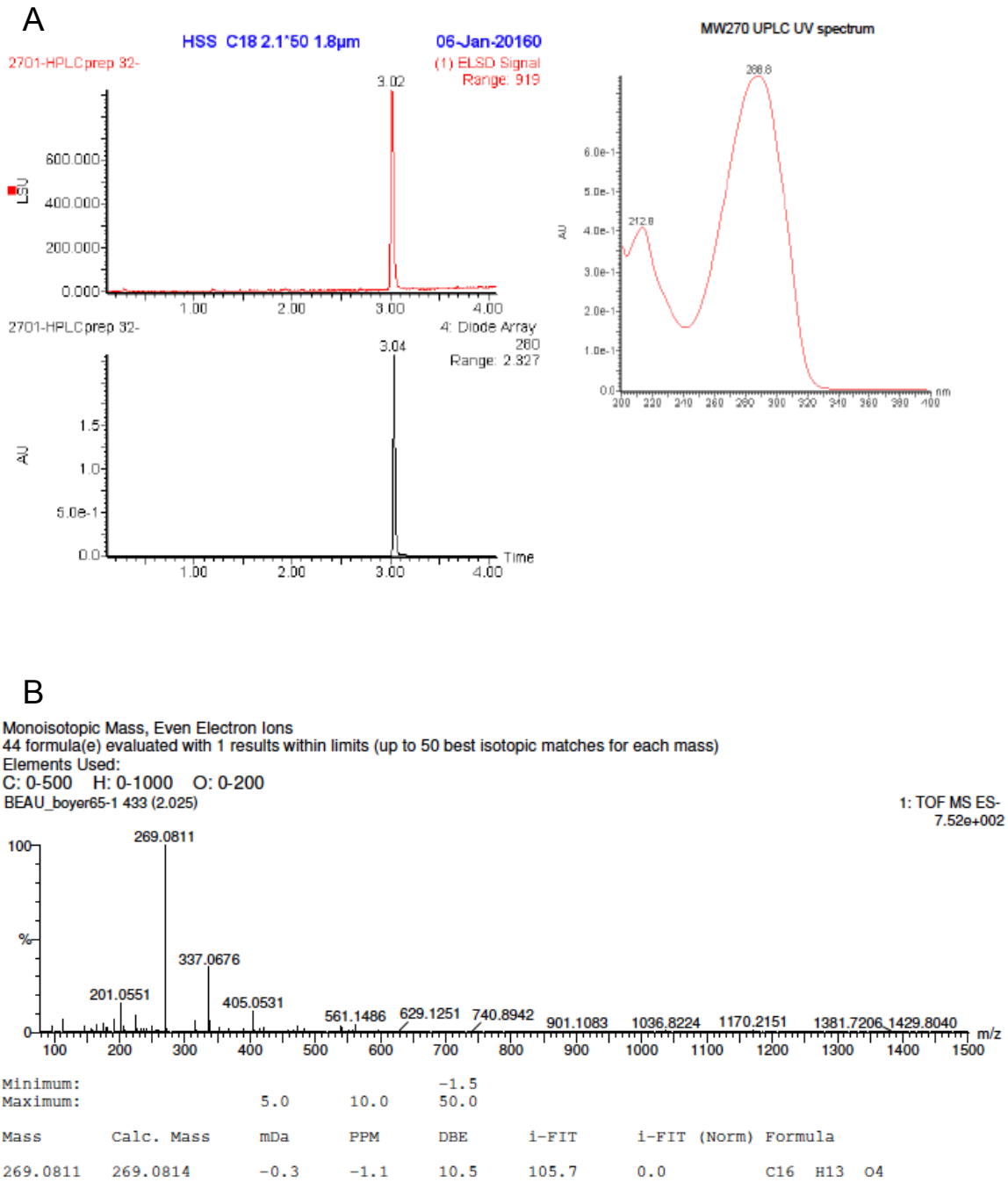

Supplementary Figure 6. (**A**) HPLC analysis of P270 after preparative HPLC purification and UV spectrum of P270. **(B)** High Resolution Mass Spectrometry (HRMS) spectrum of P270 (negative mode).

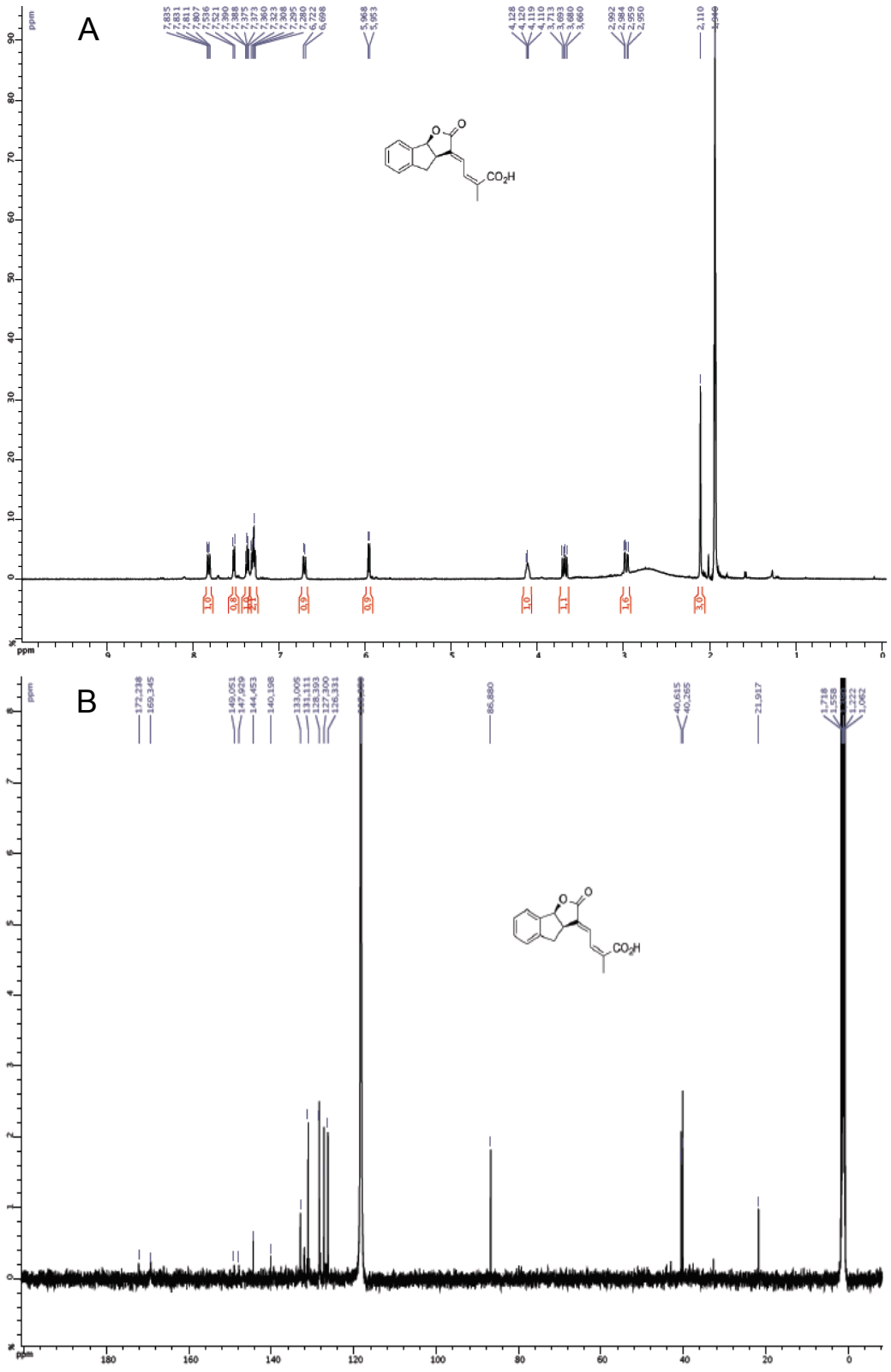

Supplementary Figure 7. (**A**) ^{1}H NMR spectrum of P270, (**B**) ^{13}C NMR spectrum of P270.

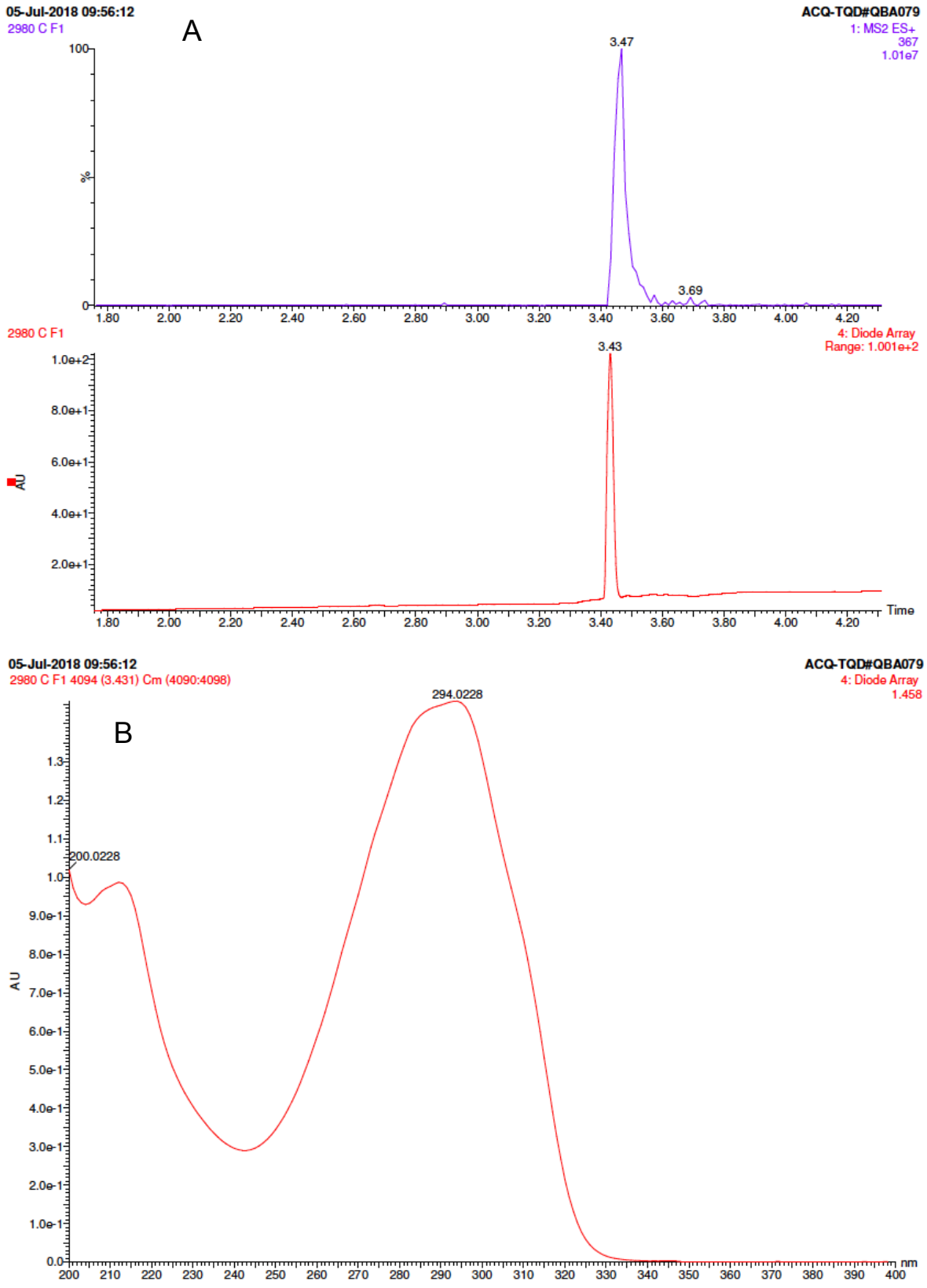

Supplementary Figure 8. (**A**) HPLC analysis of (±)-contalactone after preparative HPLC purification and (**B**) UV spectrum of (±)-contalactone.

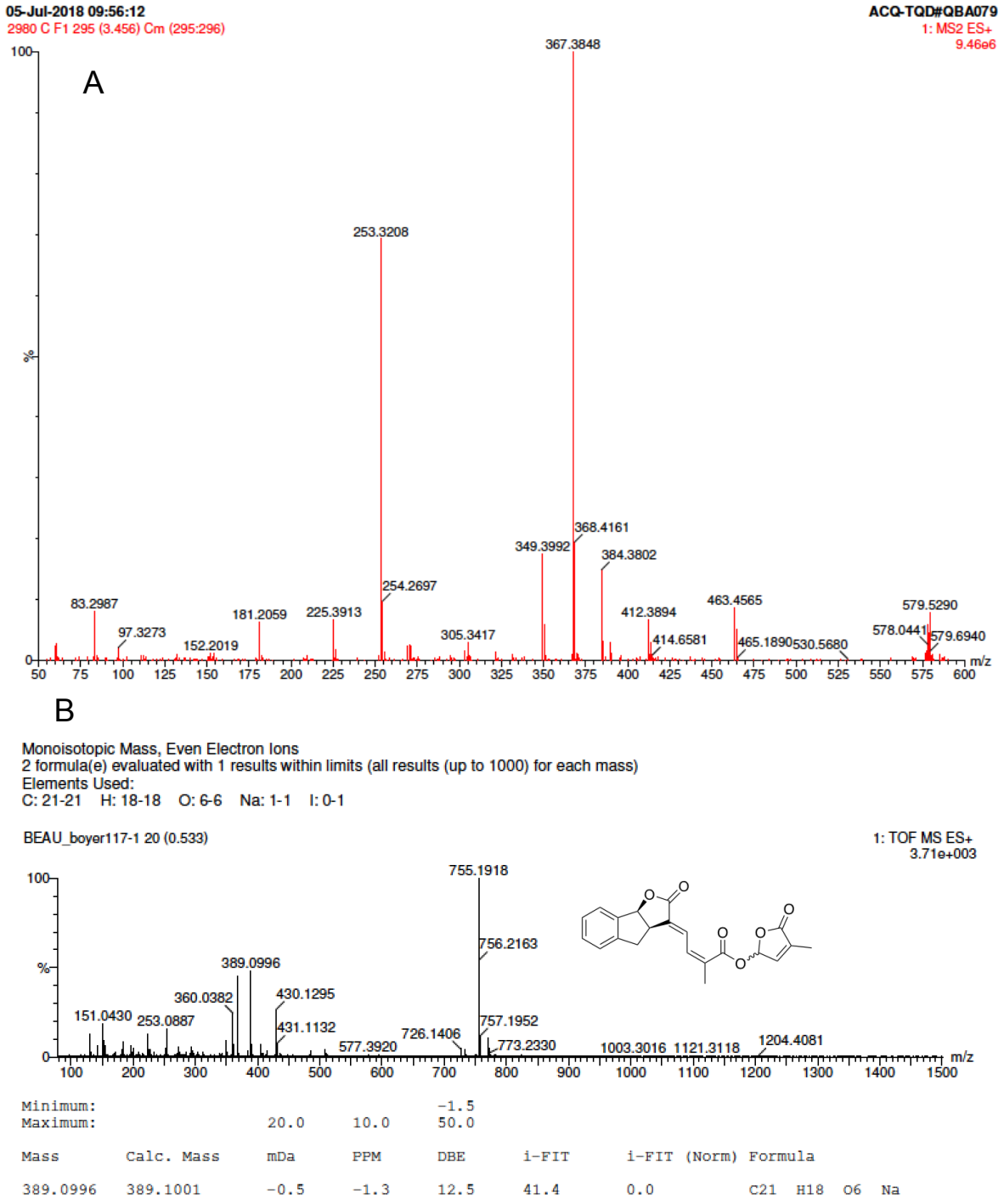

Supplementary Figure 9. (**A**) MS spectrum and (**B**) High Resolution Mass Spectrometry (HRMS) spectrum of (±)-contalactone (positive mode).

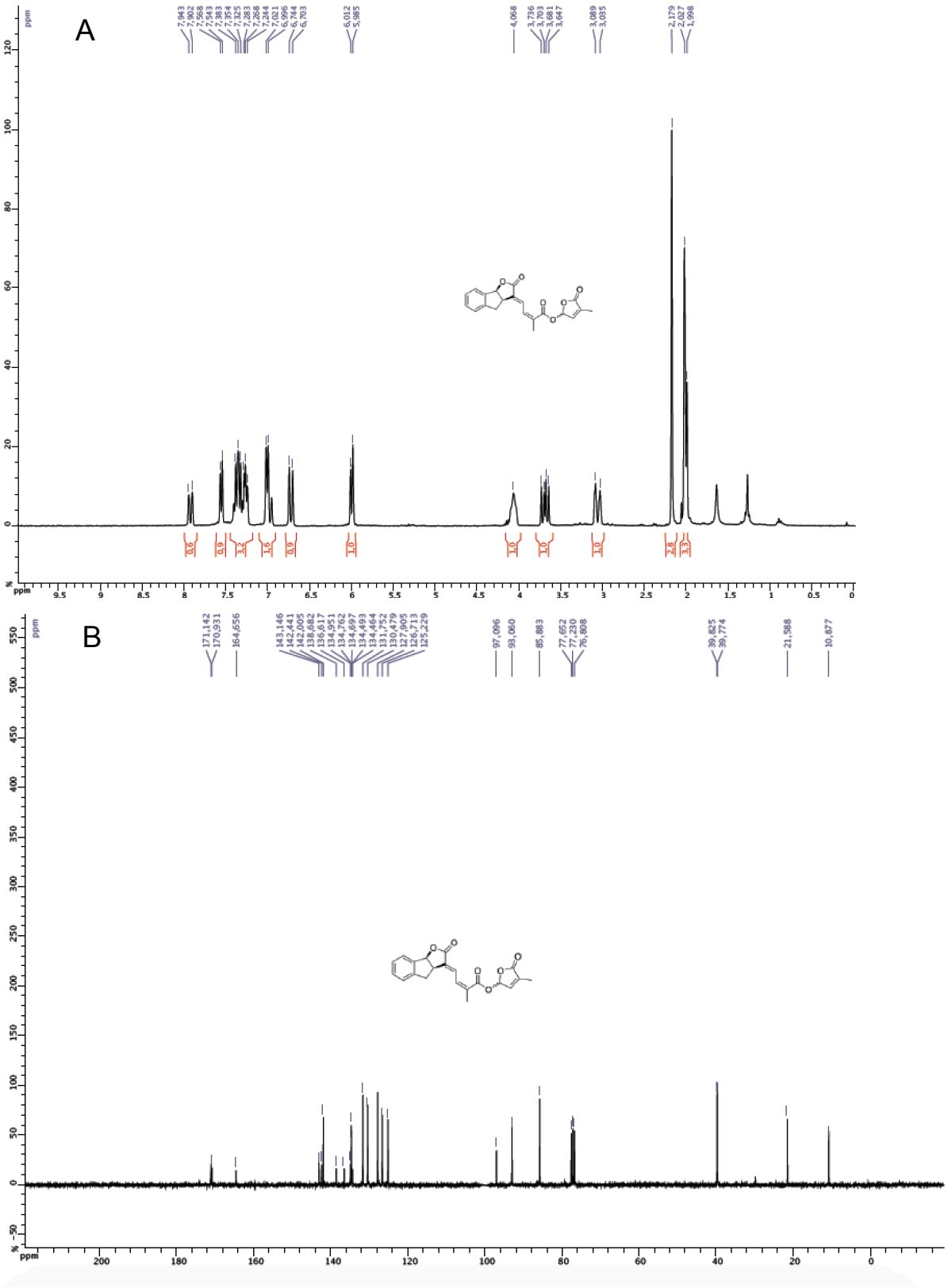

Supplementary Figure 10. (**A**) ^{1}H NMR spectrum of (±)-contalactone and (**B**) ^{13}C NMR spectrum of (±)-contalactone.

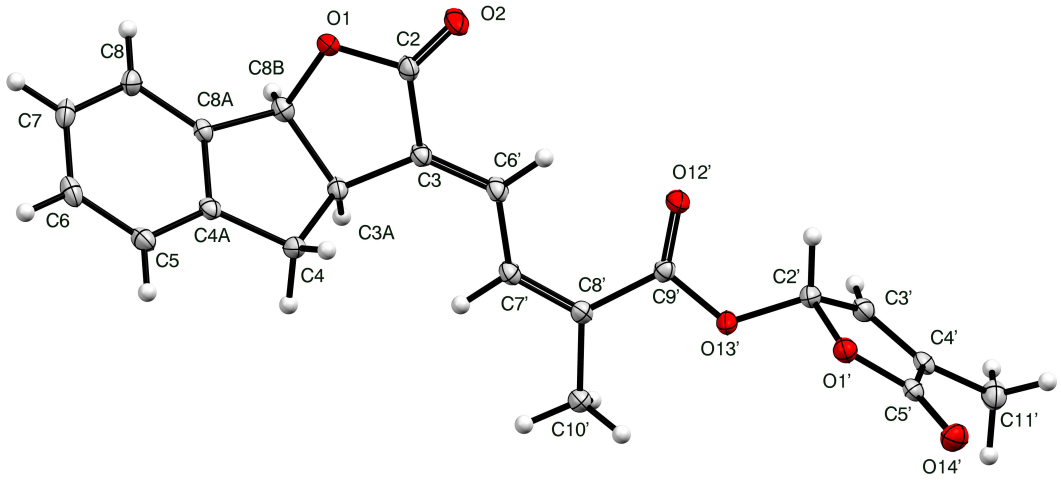

Supplementary Figure 11. An ORTEP plot of (±)-contalactone (FDB2980F1) showing one copy of the monoclinic asymmetric unit. Ellipsoids are drawn at the 30% probability level and H atoms are shown as small spheres of arbitrary radii.

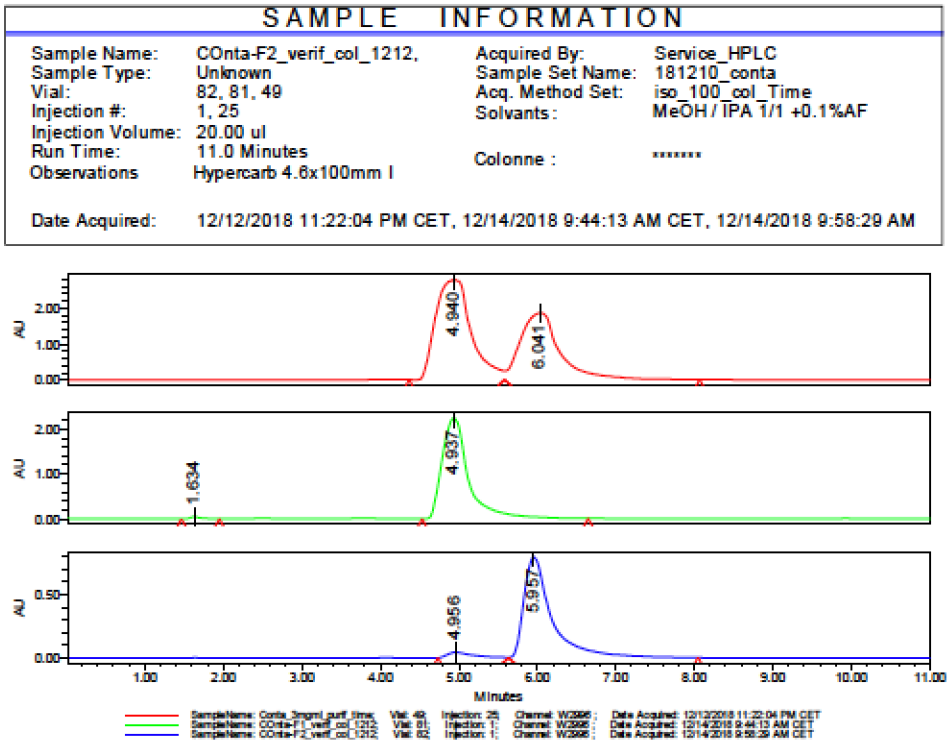

Processed Channel: W2996 PDA 289.0 nm (PDA 200.0 to 400.0 nm at 2.4 nm)

	Processed Channel	Retention Time (min)	Area	% Area	Height
1	W2996 PDA 289.0 nm (PDA 200.0 to 400.0 nm at 2.4 nm)	1.634	403042	0.76	45855
2	W2996 PDA 289.0 nm (PDA 200.0 to 400.0 nm at 2.4 nm)	4.937	52465538	99.24	2237666
3	W2996 PDA 289.0 nm (PDA 200.0 to 400.0 nm at 2.4 nm)	4.956	940638	4.59	41831

Processed Channel: W2996 PDA 289.0 nm (PDA 200.0 to 400.0 nm at 2.4 nm)

	Processed Channel	Retention Time (min)	Area	% Area	Height
4	W2996 PDA 289.0 nm (PDA 200.0 to 400.0 nm at 2.4 nm)	5.957	19549555	95.41	795510
5	W2996 PDA 289.0 nm (PDA 200.0 to 400.0 nm at 2.4 nm)	4.940	87830343	57.50	2779269
6	W2996 PDA 289.0 nm (PDA 200.0 to 400.0 nm at 2.4 nm)	6.041	64916628	42.50	1860436

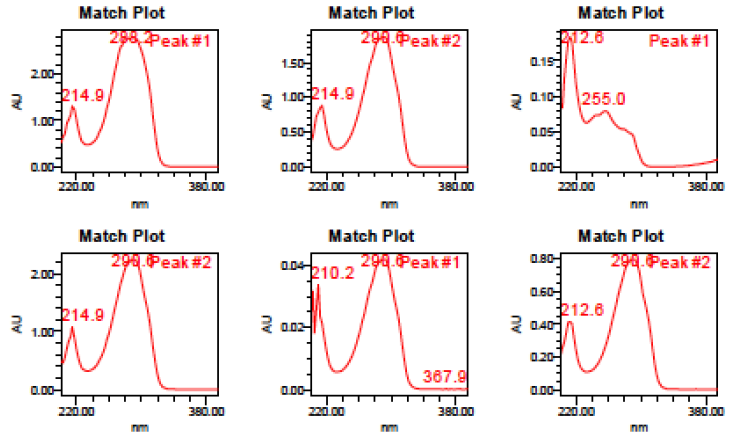

Supplementary Figure 12. HPLC separation of both diastereomers of (±)-contalactone.

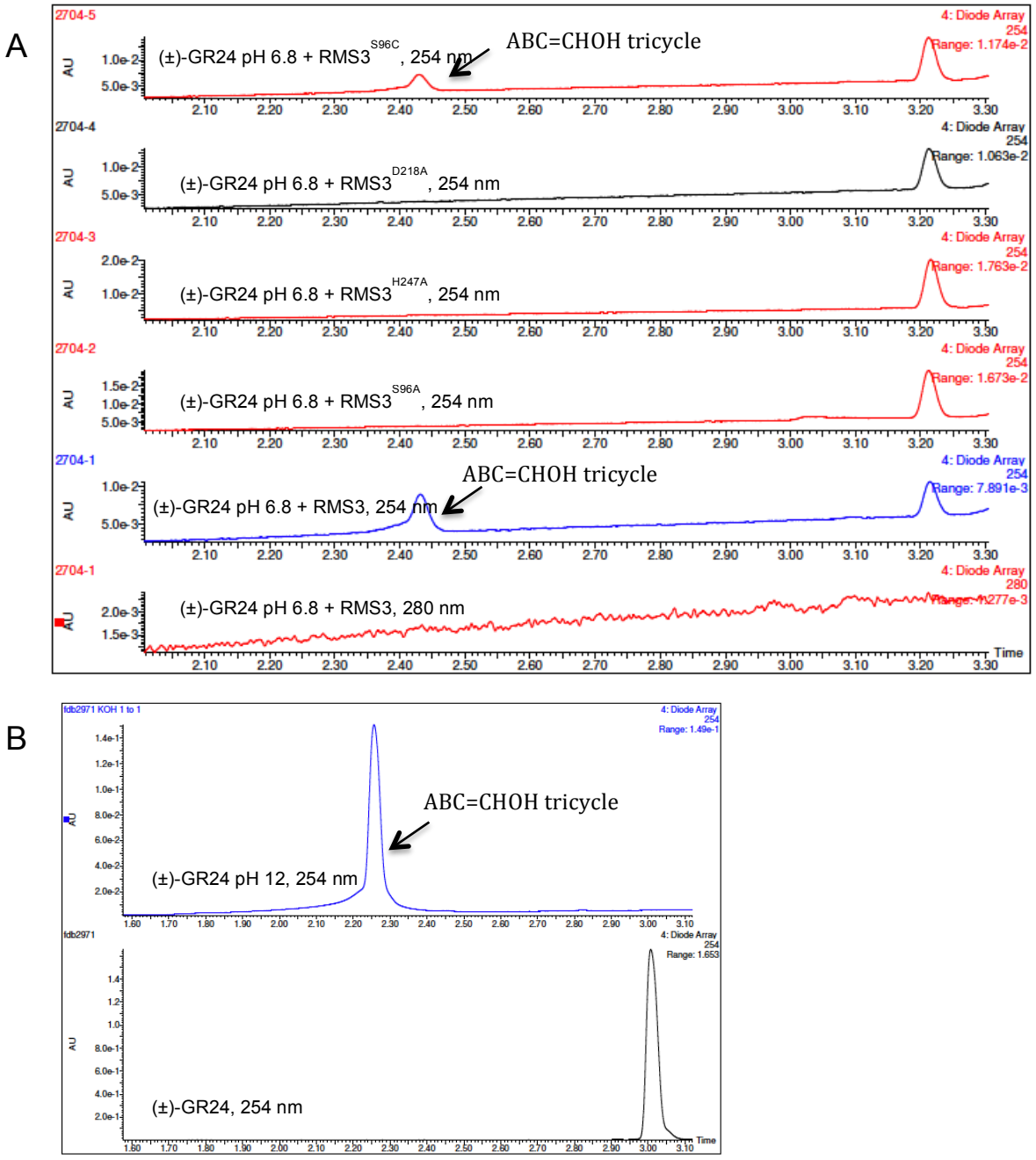

Supplementary Figure 13. Elution profile of the enzymatic assay (**A**) with buffer (pH 6.8), RMS3, RMS3^{S96A}, RMS3^{H247A}, RMS3^{D218A}, RMS3^{S96C} and the chemical assay (**B**) (KOH, pH 12) with (±)-GR24 obtained by careful purification with preparative HPLC. UPLC with diode array detection (254, 280 nm) shows the formation of ABC=CHOH and no compound P270.

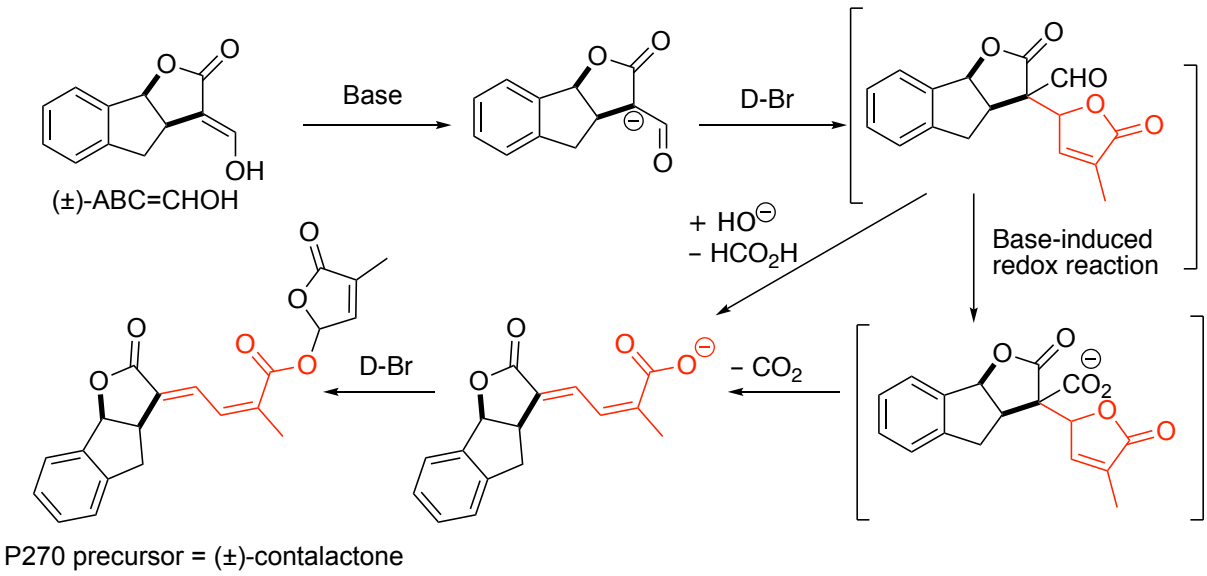

Supplementary Figure 14. Proposed mechanism for the formation of (±)-contalactone (P270 precursor).

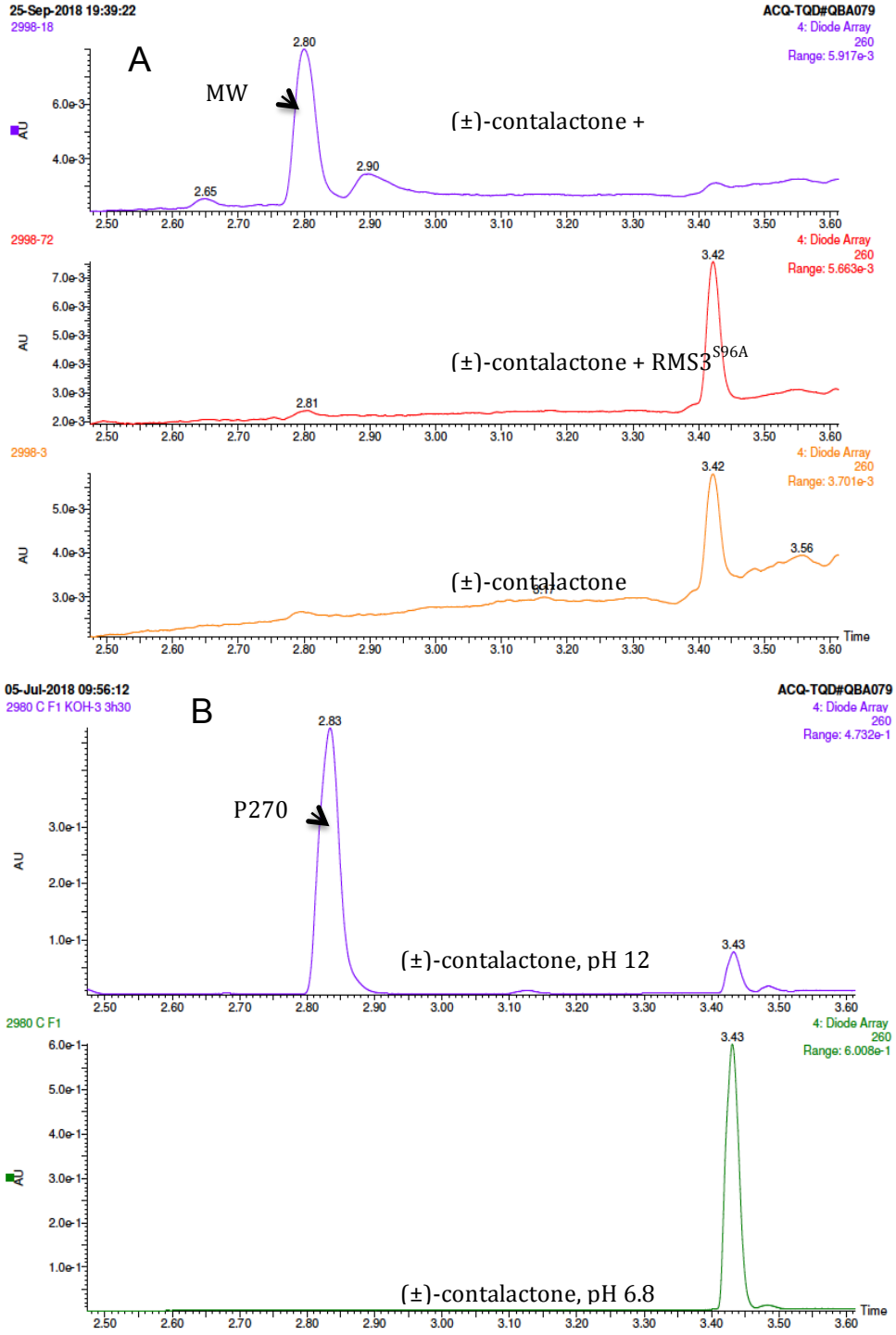

Supplementary Figure 15. Elution profile of the enzymatic assay (**A**) in buffer (pH 6.8), with RMS3, RMS3^{S96A} and chemical assay (**B**) (KOH, pH 12) with (±)-contalactone obtained by careful purification by preparative HPLC. UPLC with diode array detection (260, 280 nm) shows the formation of P270.

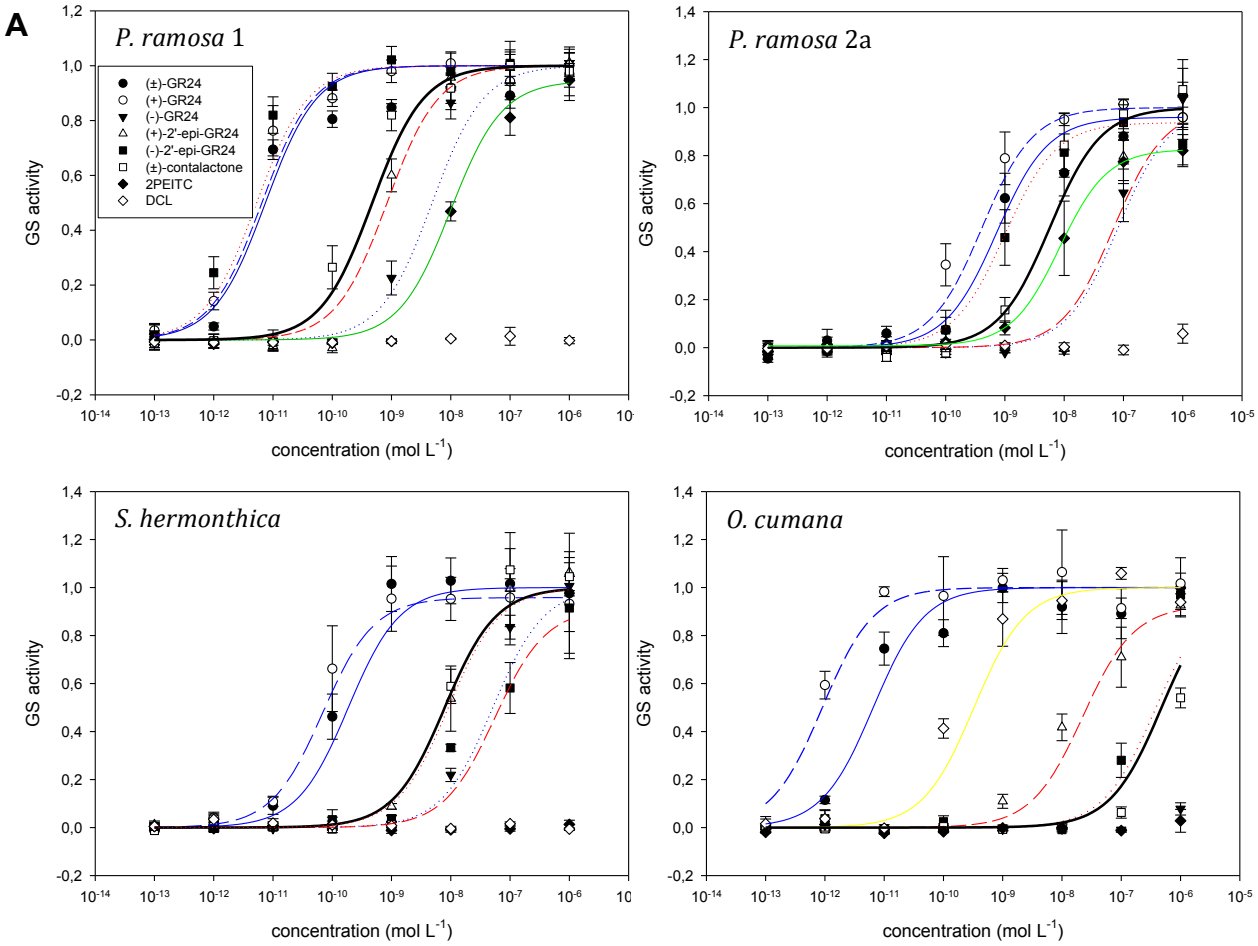

Supplementary Figure 16. Germination Stimulation (GS) activity on seeds of *P. ramosa, O. cumana* and *S. hermonthica* by (±)-contalactone. Comparison with GR24 isomers, dehydrocostus lactone (DCL) and 2-phenethyl isothiocyanate (2-PEITC). Dose response activities and modeled curves of (±)-GR24 blue; (+)-GR24 dash blue; (−)-GR24 dot blue; (+)-2'-*epi*-GR24 dash red; (−)-2'-*epi*-GR24 dot red; (±)-contalactone black; 2-PEITC green; DCL yellow.

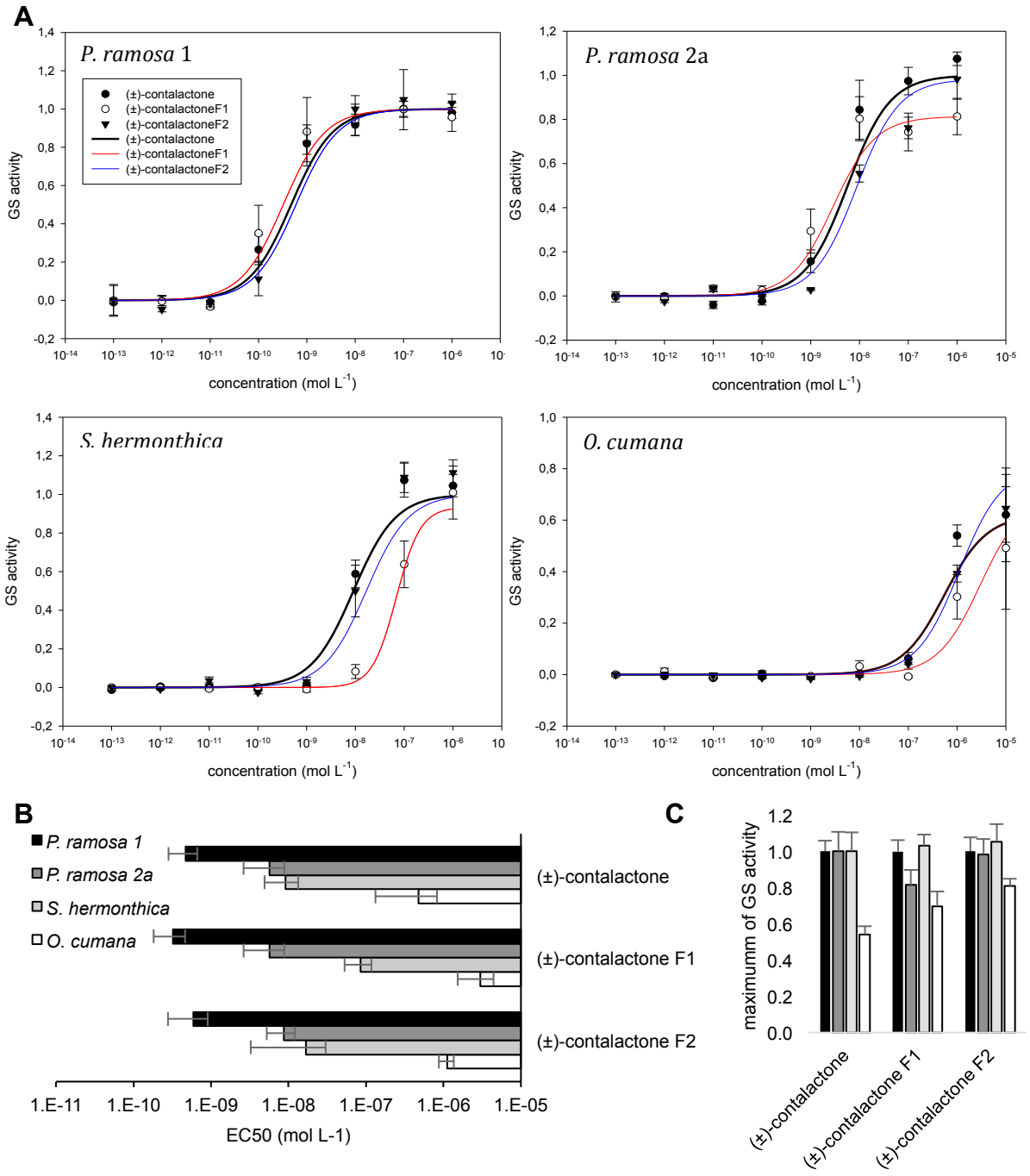

Supplementary Figure 17. Germination Stimulation (GS) activity on seeds of *P. ramosa, O. cumana* and *S. hermonthica* by (±)-contalactoneF1, (±)-contalactoneF2 and (±)-contalactone. (**A**) Dose response GS activities and modeled curves. **(B)** EC_{50} (half maximal effective concentration) (mol.L^{-1}) (**C**) Maximum of GS activity relative to (±)-GR24 (1 µM). Data are presented ± SE. (±)-contalactone = (±)-contalactoneF1 + (±)-contalactoneF2 (1:1).

Reference:

Mangnus, E.M., Dommerholt, F.J., Dejong, R.L.P. and Zwanenburg, B. (1992) Improved Synthesis of Strigol Analog GR24 and Evaluation of the Biological-Activity of Its Diastereomers. *J. Agric. Food. Chem.*, **40**, 1230-1235.